The effects of AAV-mediated XIAP gene therapy in a mouse model of glaucoma

Shagana Visuvanathan

January 14, 2019

Thesis submitted to the Faculty of Graduate and Postdoctoral Studies
in partial fulfillment of the requirements for the
MSc. degree in Biochemistry

Department of Biochemistry, Microbiology and Immunology

Faculty of Medicine

University of Ottawa

ABSTRACT

Glaucoma is a prevalent retinal neurodegenerative disease that is characterized by progressive visual field loss, leading to eventual blindness. The main risk factor for glaucoma is elevated intraocular pressure (IOP) which results in the damage and death of retinal ganglion cells (RGCs) and their axons. The endpoint of the disease is the death of these cells by apoptosis; therefore, blocking the activation of apoptosis was hypothesized to be an effective therapy. Magnetic microbeads were injected into the eyes of mice to induce a model of ocular hypertension. Apoptosis was targeted through viral-mediated ocular delivery of the X-linked inhibitor of apoptosis (XIAP) gene, a potent caspase inhibitor. XIAP overexpression resulted in significant protection of ganglion cell somal and axonal function in glaucomatous eyes, and their optic nerves showed preservation of axon density, counts, and myelination, suggesting XIAP was able to provide both structural and functional protection. The results of these experiments provide proof-of-principle for XIAP's efficacy as a neuroprotective treatment for glaucoma and are an important step forward in evaluating its full therapeutic potential.

TABLE OF CONTENTS

LIST OF FIGURES

CHAPTER 1: INTRODUCTION

CHAPTER 2: MATERIALS AND METHODS

CHAPTER 3: RESULTS

ABBREVIATIONS

AAV	Adeno-associated virus
AAV2/2	Adeno-associated virus type 2 serotype 2
AH	Aqueous humour
Apaf-1	Apoptotic protease-activating factor 1
ARVO	Association for Research in Vision and Ophthalmology
BAK	Bcl-2-antagonist/killer
BAX	Bcl-2-associated X protein
BCL	B-cell lymphoma
BDNF	Brain-derived neurotrophic factor
BIR	Baculovirus IAP repeat
B.N.P.	Bacitracin, neomycin, polymyxin B
BSA	Bovine serum albumin
BSS	Balanced salt solution
CBA	Chicken beta actin
$cd.s/m^2$	Candela second per meter squared
CMV	Cytomegalovirus
DAPI	4',6-diamidino-2-phenylindole
ERG	Electroretinography
GCL	Ganglion cell layer
GFP	Green fluorescent protein
H&E	Hematoxylin and eosin
HA	Hemagglutinin
IAP	Inhibitor of apoptosis
INL	Inner nuclear layer
IOP	Intraocular pressure
LC	Lamina cribrosa
LGN	Lateral geniculate nucleus

LHON	Leber's hereditary optic neuropathy
NF-κB	Nuclear factor kappa B
NTG	Normal tension glaucoma
ON	Optic nerve
ONL	Outer nuclear layer
ONH	Optic nerve head
PACG	Primary angle-closure glaucoma
PBS	Phosphate buffered saline
PERG	Pattern electroretinography
PFA	Paraformaldehyde
POAG	Primary open-angle glaucoma
RING	Really interesting new gene
RGC	Retinal ganglion cell
RNFL	Retinal nerve fibre layer
ROS	Reactive oxygen species
RT	Room temperature
SOD	Superoxide dismutase
TEM	Transmission electron microscopy
TM	Trabecular meshwork
TNF-α	Tumor necrosis factor alpha
VEP	Visual evoked potentials
WN1316	2-[mesityl(methyl)amino]-N-[4-(pyridin-2-yl)-1H-imidazol-2-yl] acetamide trihydrochloride
WPRE	Woodchuck hepatitis virus posttranscriptional regulatory element
XAF-1	XIAP-associated factor 1
XIAP	X-linked inhibitor of apoptosis

Dedicated to Ammamma,

my most cherished well-wisher and friend.

ACKNOWLEDGEMENTS

I would first like to thank my supervisor, Dr. Catherine Tsilfidis for giving me this opportunity. Thank you for all your help throughout this project, and for allowing me to make it my own. You have always made yourself available and approachable, and I cannot thank you enough for such a rewarding experience.

I would also like to express my sincere gratitude to Adam Baker and Dr. Pamela Lagali. Adam, thank you for always being willing to help me with anything during the course of my studies, including the surgeries and especially the electrophysiology. Pam, you are a wealth of knowledge and a fantastic teacher; thank you for always being open to answering any and all questions. Both of you were endlessly supportive and patient, and made the work in this thesis possible. Thank you for being the greatest mentors a student could ask for.

It was a pleasure to have Dr. Robert Korneluk and Dr. Stuart Coupland as my Thesis Advisory Committee members. Thank you for your guidance and support throughout this process. I would also like to thank Jeff McClintock for invaluable help with the optic nerve histology, as well as Dr. Gary Miller for his insight on glaucoma throughout the experiments.

To all my wonderful labmates and the people I befriended, thank you for making my time in Ottawa such a positive experience. I have enjoyed getting to know each and every one of you, and I wish you all the success in the world. A special thank you to Neethu Govindaraju, and John Girgis. Neethu, thank you for being an amazing roommate and an even better friend. John, I would not have gotten this far without your continuous enthusiasm, encouragement, and good humour. Thank you for everything you've done for me these past couple of years, and for always being there for me without fail.

Lastly, to Amma and Appa. Thank you for helping me at every step of this journey and for being my staunchest supporters. Regardless of what you were going through, when I faced problems of my own, you were always willing to forget your troubles to support me in facing mine. Thank you for always finding the silver lining in every situation and for helping me persevere through hardships and failure. None of my accomplishments would have been possible without everything you've done for me.

Thank you.

1.0 INTRODUCTION

1.1 The Eye

1.1a The Humours

The human eye is a complex organ composed of several different cell types. It is divided into two segments: the anterior segment, and the posterior segment, each of which is filled with fluid to help maintain the rigidity of the eye. The anterior segment is composed of the anterior and posterior chambers, containing the cornea, sclera, iris, trabecular meshwork, lens, and ciliary body, and is filled with aqueous humour. Aqueous humour (AH) is a transparent fluid that is responsible for providing nutrients to avascular ocular tissues such as the cornea and the lens, and is continually produced and drained to maintain visual clarity (Goel et al., 2010). The humour is secreted from the ciliary body and travels from the posterior chamber to the anterior chamber through the pupil to eventually drain into the trabecular meshwork (TM), a spongy network of connective tissue that filters the fluid before it exits through the episcleral veins to join the bloodstream (Goel et al., 2010). The trabecular meshwork and scleral outflow pathways are located at the iridocorneal angle, the junction at which the iris and cornea meet.

The posterior segment is composed of the vitreous chamber, which is filled with a gelatinous, transparent mass called the vitreous humour. The vitreous is also produced by the ciliary body and attaches to the lens on one side, and the retinal vessels on the other side. It is composed of hyaluronic acid and various types of collagen in order to give it its consistency (Donati et al., 2014). Unlike the aqueous humour, the vitreous humour is not repeatedly replenished. The introduction of blood cells and other

molecules can therefore remain in the vitreous, impeding vision, and can only be removed through surgical intervention (Donati et al., 2014).

1.1b The Retina

The vertebrate retina is a thin, transparent layer of tissue responsible for converting light into visual information to be processed in the brain. It develops from the optic cup as an outgrowth of the forebrain, with the inner segment forming the retina and the outer segment forming the retinal pigment epithelium (RPE), which is attached to the choroid (Sinn and Wittbrodt, 2013).

The retina is composed of several classes of neurons, arranged into three parallel nuclear layers: the outer nuclear layer (ONL), the inner nuclear layer (INL), and the ganglion cell layer (GCL) (Figure 1.1). These layers are connected via synapses that form two plexiform layers: the outer plexiform layer, and the inner plexiform layer. The ONL is composed of the nuclei of the photoreceptors (rods and cones), which are responsible for converting the light input into electrical signals that are transmitted through synapses formed with the interneurons (bipolar, horizontal, and amacrine cells), whose nuclei make up the INL (Masland, 2012). The interneurons then propagate the signalling onto the retinal ganglion cells (RGCs) in the GCL, which also contains displaced amacrine cells. These RGCs extend axons that compose the retinal nerve fibre layer (RNFL), and project through the optic disc to form the optic nerve, which is responsible for the transmission of information to the visual cortex of the brain (Masland, 2012).

1.1c The Optic Nerve

The optic nerve is the sole method of transmission from the retina to the brain and is therefore a key component of the visual pathway. It begins in retina and ends at the lateral geniculate nucleus (LGN)

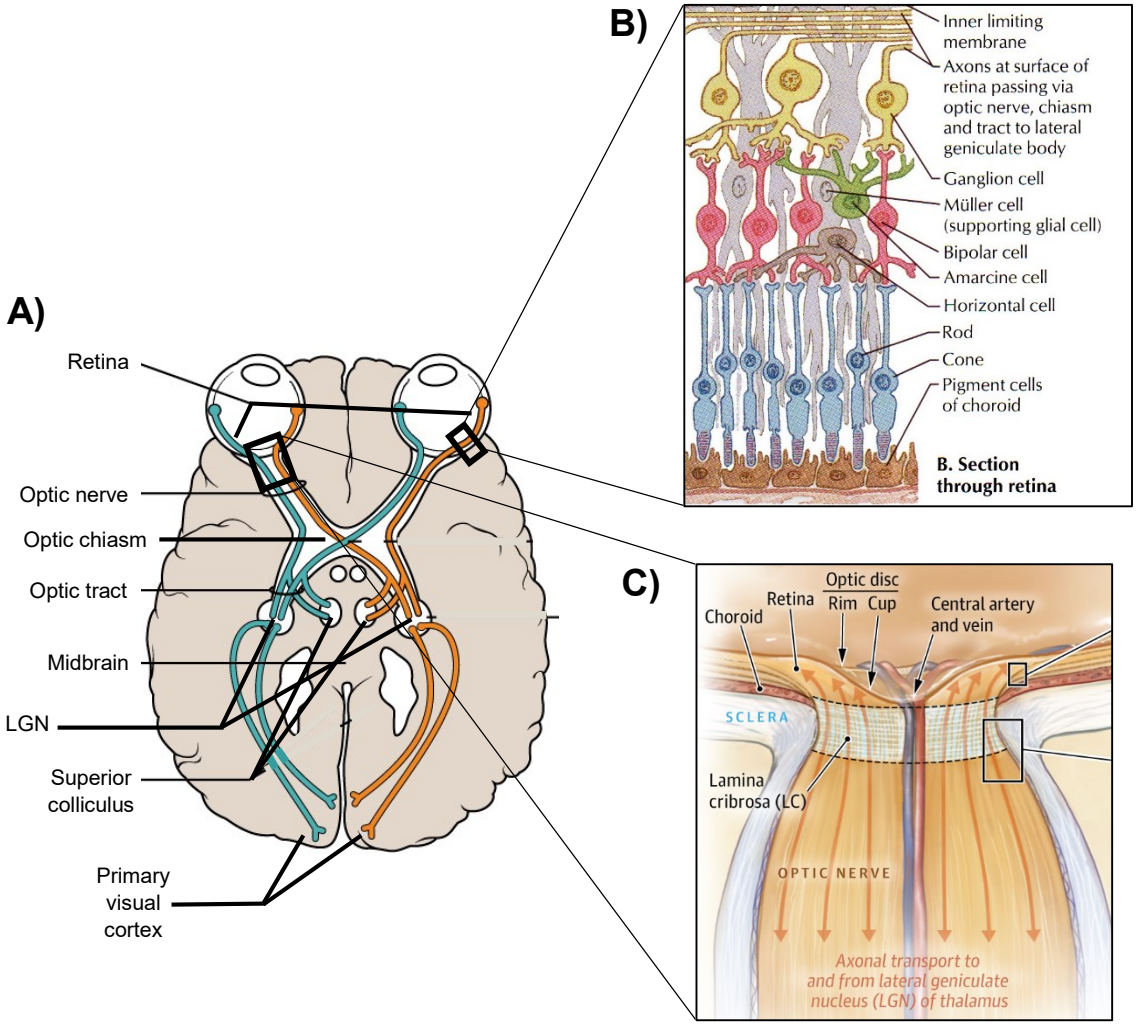

Figure 1.1. Diagram of the visual pathway. a) The visual pathway starts with the retina, which sends information to its primary target, the lateral geniculate nucleus (LGN), via the optic nerve. The LGN relays the signal to the visual cortex of the brain, where the pathway ends. **b)** The neural retina resides at the posterior end of the eye and is a multi-layer structure composed of neurons, glia, synapses, and epithelial tissue. Rod and cone photoreceptors receive light and transmit the signal to the interneurons, who modulate the information and send it to the retinal ganglion cells (RGC). **c)** RGCs extend axons that compose the retinal nerve fibre layer, and travel through the optic disc and lamina cribrosa to form the optic nerve. The axons intersect at the optic chiasm and diverge to continue to the LGN, which transmits the information to the visual cortex. Figures adapted from (Gaillard; Weinreb et al., 2014). Image of retina obtained from Netter medical illustrations with permission of Elsevier. All rights reserved.

in the thalamus, and is composed of both RGC axons and glial cells (Figure 1.1). Glial cells synthesize growth factors and trophic factors to provide nutrients to the axons, and also provide structural support by extending projections to connect to other glial cells and hold the nerve bundles in place (Hernandez, 2000). Ganglion cell axons extend towards the optic disc and turn at a 90° angle to exit the eye. As the axons turn, they enter the prelaminar region where they are bundled into axon fascicles by glial cells (Anderson, 1969). These fascicles continue by passing through the lamina cribrosa (LC), a sieve-like network composed of approximately 10 layers of porous connective tissue and glial cells that supplies the unmyelinated nerve with nutrients and support (Anderson, 1969). The axons pass through LC, entering the retrolaminar region, where oligodendrocytes produce myelin to sheath the axons as they exit the globe. The myelinated axons continue along the nerve until they reach the optic chiasm, where the majority of the axons cross over to extend contralaterally while the remaining fibres continue to travel ipsilaterally (Erskine and Herrera, 2014) (Figure 1.1a). A number of the fibres terminate at the LGN, the primary visual target in higher mammals which projects to the visual cortex, while the other axons extend to the superior colliculus, the secondary visual target involved in movement detection (Erskine and Herrera, 2014).

1.2 Glaucoma

1.2a Overview

Glaucoma is a collection of optic neuropathies that eventually results in complete blindness, usually starting with peripheral vision loss. It is a leading cause of irreversible blindness worldwide, second only to age-related macular degeneration, with over 70 million people currently affected, 10% of whom are bilaterally blind (Quigley and Broman, 2006). It is predicted to affect 76 million people by 2020,

which is estimated to increase to 111.8 million by 2040 (Tham et al., 2014). Glaucoma is often asymptomatic until it is too severe, thereby going unnoticed by many individuals who are affected, primarily due to its manifestation in elderly patients. Studies suggest only 10-50% of glaucoma patients are aware that they have the disease, and symptoms are not evident until patients are older (Hennis et al., 2007; Sathyamangalam et al., 2009). Many age-related diseases have known associations with glaucoma, including hypertension, hypotension, diabetes and cataracts; the accumulation of these health deficits can increase frailty and increase the chances of developing glaucoma (McMonnies, 2017).

1.2b Primary Open-Angle Glaucoma (POAG)

The most common form of glaucoma is primary open-angle glaucoma (POAG), an asymptomatic condition characterized by progressive visual field loss which is responsible for more than 85% of diagnosed cases. It typically manifests in patients over the age of 50, with a worldwide prevalence of 3.54% (Tham et al., 2014).

There are several risk factors for POAG, including genetics, family history, and racial background. Many genes have been identified in association with glaucoma development; however, genetic causation only accounts for 10% of all glaucoma cases. One of the first genes to be identified was the *MYOC* gene, which is located on chromosome 1 and encodes the protein myocilin (Stone et al., 1997). Although the mechanisms of myocilin-related glaucoma are not fully understood, patients with disease-introducing mutations develop early-onset POAG with extremely high IOPs. Adult populations of POAG carry mutations around 3-5% of the time, and mutation carriers develop the disease almost 90% of the time (Kwon et al, 2009). There is also a familial association for glaucoma development. Approximately 50% of all POAG patients have a positive family history for the disease. Immediate family members of glaucoma

patients have an increased risk of up to nine-fold to develop glaucoma than the average individual, with a lifetime risk of 22% (Wolfs et al., 1998). Another main risk factor is race. Population studies revealed that in certain age ranges, black Americans were six times more likely to develop POAG than white populations; however, white populations had the sharpest increase in POAG development with age (Rudnicka et al., 2006).

Although glaucoma pathogenesis is not completely understood, it is clear that one of its main risk factors is elevated intraocular pressure (IOP), defined as a pressure greater than 21 mmHg in patients. IOP changes are caused by an upset in the secretion and drainage balance of the aqueous humour in the anterior portion of the eye. Patients with POAG exhibit increased resistance of AH drainage through its outflow pathways at either the trabecular meshwork or the episcleral veins. As previously mentioned, AH is constantly produced to fill the anterior chamber and mostly drained through the trabecular meshwork pathway. Outflow resistance is primarily regulated by the trabecular meshwork; TM cells are capable of maintaining homeostasis in outflow resistance to counter regular fluctuations in IOP by modulating the expression levels of various components of the network (Acott et al., 2014). However, abnormal development or TM cell damage can result in structural deficits that can significantly impact drainage. During fetal development, TM morphogenesis is largely completed, resulting in a mass of mesenchymal cells (Johnston et al., 1979). These cells differentiate postnatally, covering extracellular matrix fibres which accumulate and reorganize to form trabecular beams and sheets (Acott and Kelley, 2008). Functional TM maturation requires the formation of inter-trabecular spaces between these structural components, which get less porous as the meshwork continues towards Schlemm's Canal (Abu-Hassan et al., 2014). It is known that the entryway of the TM is composed of cells that are highly phagocytic; AH collects debris along the way which must be eliminated efficiently to prevent blockages (Lütjen-Drecoll, 1999; Abu-

Hassan et al., 2014). Changes in TM porosity and integrity, or deficiencies in particle elimination can result in increased outflow resistance and lead to AH buildup in the anterior cavity. Because the eye is a closed system, pressure elevation in the anterior chamber leads to pressure throughout the eye, resulting in degeneration and death of retinal ganglion cells and the optic nerve. The mechanisms of this damage will be discussed later in this chapter.

1.2c Primary Angle-Closure Glaucoma (PACG)

Although primary angle-closure glaucoma (PACG) is much less prevalent than POAG, it is also three times more likely to result in severe bilateral visual impairment (Quigley and Broman, 2006; Tham et al., 2014). While POAG is a chronic disease that slowly progresses, PACG originates as an acute attack, which can progress to a chronic disease if immediate medical intervention doesn't occur. PACG is caused by direct blockage of the iridocorneal angle, either by the iris or by adhesional angle closure (Weinreb et al., 2014). Instead of increased resistance in AH outflow, acute PACG results in a complete inhibition of AH drainage, causing an immediate and very high IOP elevation. Chronic PACG is also a variation, where the iris gradually covers the trabecular meshwork, resulting in IOP elevation (Sun et al., 2017). The onset of acute PACG is often accompanied by ocular pain, dizziness, nausea, and headaches, which will prompt patients to seek treatment. However, chronic PACG operates much like POAG and is asymptomatic and painless in the early stages because the eye gradually gets used to the slowly increasing IOP. Patients are unaware of the disease onset until vision loss begins.

PACG has a disease pathophysiology unique enough from POAG that it is associated with its own set of risk factors, with the exception of age and elevated IOP. PACG is more prevalent in females, unlike POAG which does not show a clear gender association for development (Amerasinghe et al., 2011). It is

also more prevalent in Asia, with over 77% of cases diagnosed in the continent (Amerasinghe et al., 2011); Chinese, Mongolian, and Eskimo populations are particularly susceptible (Sun et al., 2017). These populations share a heritable anatomical risk factor: shallow anterior chamber depth, which increases the chances of iris closure over the angle (Nongpiur et al., 2011). Genome-wide association studies with 1,854 PACG patients and over 8,000 control patients from Asia have identified three different loci that are strongly associated with disease susceptibility at rs11024102 (*PLEKHA7*, chromosome 11), rs3753841 (*COL11A1*, chromosome 1), and rs1015213 (located between *PCMTD1* and *ST18*, chromosome 8q) (Vithana et al., 2012). These genes are not associated with POAG, suggesting that both PACG and POAG are genetically distinct diseases.

1.2d Normal Tension Glaucoma (NTG)

Normal tension glaucoma (NTG) is a subset of POAG unique to the glaucoma family in that it doesn't share the main risk factor: higher-than-average IOP. Interestingly, it still exhibits the same clinical signs and disease pathology as the other forms. With high-IOP glaucomas, the initial insult is known to be ocular hypertension, resulting in stress-induced neurodegenerative damage. However, in a glaucomatous disease where IOP is irrelevant, it is difficult to establish the mechanisms of pathogenesis.

A variety of hypotheses have been developed, none of which have been able to provide a definitive explanation NTG, suggesting that NTG has a multifactorial pathophysiology. The most popular theory is that patients with NTG are less tolerant to lower IOPs; pressure tolerance varies amongst population groups and those that are more susceptible could experience a similar pathophysiology to high tension glaucoma patients with average IOPs (Collaborative Normal-Tension Glaucoma Study Group, 1998). NTG is more prevalent in Asia, accounting for anywhere from 52-92% of all glaucoma cases depending

on the country and the age group (Cho and Kee, 2014), whereas the incidence in Caucasian populations was only 30-39% of studies (Klein et al., 1992), suggesting that there may be a genetic component associated with variable susceptibility. There have been reports of mutations in the *OPTN* gene, encoding optineurin, in glaucoma patients, predominantly in patients with NTG (Rezaie et al., 2002). The protein is reportedly expressed in the retina, trabecular meshwork, ciliary body, and brain. Optineurin's function has not yet been elucidated, although it has been implicated in the tumor necrosis factor alpha (TNF-α) pathway, and is hypothesized to have neuroprotective abilities (Rezaie et al., 2002).

1.3 Mechanisms of Glaucomatous Damage

The pathophysiological mechanisms of glaucomatous optic neuropathy are still not well-understood. However, a widely-accepted theory is that ocular hypertension leads to stress-induced degeneration of the retina and the optic nerve.

Elevated IOP can result in mechanical stress against the structures of the posterior eye. The lamina cribrosa (LC), where the axon bundles exit through, is particularly vulnerable to stress-induced damage (Quigley et al., 1981). IOP elevation leads to bowing, deformation, and remodeling of the plates, which in turn crimps and physically damages the axons that pass through, resulting in alterations in optic nerve microcirculation, loss of glial support, and disrupted axonal transport, eventually leading to degeneration of the fibres (Quigley et al., 1983). Studies have shown disruption of both anterograde and retrograde transport occur early in glaucoma, preventing vital nutrients and trophic factors from reaching their targets in the brain or the ganglion cells (Chidlow et al., 2011). Anterograde transport is required for sending important proteins and lipids from the cell body, as well as transport of mitochondria for energy in the axons (Fahy et al., 2016). Axons do not possess the necessary machinery for protein synthesis so

they rely on functional transport from the cell body for sustainment. Retrograde transport is necessary for removing misfolded protein aggregates from the axons and sending trophic signals from distal sites (Perlson et al., 2010). Deficits in axonal transport in both directions result in the accumulation of vesicles, disorganized microtubules, and protein aggregates in the laminar and prelaminar regions of the optic nerve head (ONH) (Perlson et al., 2010; Martin et al., 2006; Chidlow et al., 2011).

Obstructions in axoplasmic flow coupled with chronic mechanical stress leads to axonal degeneration. Axons begin to die near the LC, which eventually leads to thinning of the retinal nerve fibre layer (Quigley et al., 1981). As axons die, the optic cup expands, altering the cup-to-disc ratio of the ONH because of the reduction in fibres that are exiting the eye in a process specific to glaucoma known as "cupping" (Quigley et al., 1981). Axonal degeneration is irreversible. Loss of axons leads to increased gliosis, where glial cells extend processes to interact with one another and hold the optic nerve together (Sofroniew, 2009). While these glial scars provide structural support, they also impede neuroregeneration as their formation prevents neurite extension.

Axon loss coupled with impediments in nerve regeneration ultimately result in the loss of ganglion cells in the retina. RGCs lose growth factors and neurotrophic factors when retrograde transport is inhibited; IOP elevation has been shown to inhibit transport of brain-derived neurotrophic factor (BDNF), a vital neuroprotective trophic factor (Johnson et al., 1986; Thanos et al., 1989), from the brain to the retina (Quigley et al., 2000) and vice versa (Caleo et al., 2000). This cell body death occurs primarily via apoptosis, a caspase-dependent form of cell death that is also responsible for pruning RGCs postnatally (Yamaguchi and Miura, 2015). Once RGCs are lost to the disease, they cannot be regained, and the progressive death leads to the gradual vision loss that is characteristic of glaucoma.

Pressure elevation can also lead to several other events, all resulting in retinal and optic nerve damage. As previously stated, axonal transport is affected in glaucoma, thereby disrupting transport of mitochondria along the axons to sites requiring energy. Elevated pressure induces damage to mitochondria in axons at the ONH; studies have shown that certain genes are downregulated in glaucoma, increasing mitochondrial fission, which subsequently releases cytochrome c (Ju et al., 2008), an activator of extrinsic apoptosis. Mitochondrial dysfunction has been reported in POAG patients, resulting in increased level of mtDNA mutations, causing deficient respiration and reduced ATP synthesis (Lascaratos et al., 2012).

Aside from restricted ATP synthesis, mitochondrial damage can also induce oxidative stress as a result of increased reactive oxygen species (ROS) production, a potent cause of damage in many neurodegenerative diseases. Oxidative stress ensues when there is an imbalance between the level of ROS and the antioxidants in the system. When ROS levels overwhelm antioxidant defenses, the unstable free radicals can cause damage. The retina is susceptible to such damage because of chronic exposure to oxidative stress caused by lipid peroxidation, constant light exposure, and its large consumption of oxygen (Moreno et al., 2004). Ideally, the retina would be able to maintain homeostasis, but when the balance between free radicals and antioxidants is compromised, oxidative stress can dysregulate functional pathways and lead to visual impairment. Studies in animal models have shown that elevated IOP increases ROS production (Ko et al., 2005; Ferreira et al., 2010), and it is hypothesized that this production may be caused by reperfusion injury. Elevated IOP compresses ocular blood vessels, leading to vascular dysregulation. Fluctuations in IOP lead to reperfusion, and the renewed blood oxygen supply increases free radical production, overwhelming the available antioxidant pool and causing injury (Renner et al., 2017). Increased oxidative stress can directly lead to RGC degeneration. Exogenous provisions of ROS

increased caspase-independent RGC apoptosis in glaucoma models (Li and Osborne, 2008), and studies reducing ROS reported temporary inhibition of RGC apoptosis (Tezel and Yang, 2004). Oxidative stress can also directly alter glutamate levels in the retina, resulting in excitotoxicity caused by glutamate accumulation. Glutamate accumulation overstimulates NMDA receptors, leading to an influx of intracellular calcium that activates a number of downstream events, eventually resulting in RGC apoptosis (Sucher et al., 1997). In rat models of glaucoma, oxidative stress has been shown to modify proteins responsible for converting glutamate to a non-toxic form, allowing toxic glutamate to accumulate (Tezel et al., 2005). There have also been reductions in retinal glutamate transporter proteins and shuttling activity in these models (Moreno et al., 2004). Both oxidative stress and glutamate toxicity are two mechanisms of damage that have been implicated in the pathophysiology of NTG, as they are pathways that can be activated irrespective of pressure changes.

Aside from inducing injury at the posterior section of the eye, oxidative stress also plays a role at inducing damage at the trabecular meshwork. TM cells are gradually lost in glaucoma patients, and the death of these cells can inhibit aqueous humour drainage, particularly because they are responsible for adjusting to IOP fluctuations. This cell death was theorized to be induced by the generation of free radicals (Alvarado et al., 1984). Free radical production in the anterior chamber primarily occurs via oxygen metabolism aided by vascular dysregulation. Radicals formed as by-products of oxygen reduction are highly unstable and can react with any neighbouring molecules, including DNA; oxidative DNA damage is more prevalent in the TM cells of glaucoma patients than healthy controls (Izzotti et al., 2003). TM cells are naturally exposed to high levels of ROS and have the necessary enzymes to limit the free radical pool; however, the concentrations of these enzymes in TM cells decline in an age-dependent manner in glaucoma patients (De La Paz and Epstein, 1996), which could explain ROS accumulation in

the meshwork and the subsequent oxidative damage of these cells. Analysis of various oxidative stress markers in glaucomatous and non-glaucomatous patients reported significantly higher marker levels in the aqueous humour of glaucoma patients (Benoist d'Azy et al., 2016; Ferreira et al., 2010). *In vivo* studies where the authors introduced ROS into TM cells of calf eyes reported significant changes in aqueous humour drainage (Kahn et al., 1983). Expression of endothelial-leukocyte adhesion molecule 1 (ELAM-1), which is protective against oxidative stress, was shown to be upregulated in the TM cells of glaucoma patients compared to healthy controls (Wang et al., 2001). These results all suggest that increased oxidative stress and ROS accumulation contribute to alterations in TM function. IOP elevation is the primary insult in most glaucomas, but it is clear that there are multiple events that ultimately result in the disease, as evidenced by the development of glaucomas independent of IOP.

1.4 Current Therapies for Glaucoma

Retinal and optic nerve degeneration in glaucoma is irreversible, and the disease is currently incurable. Available therapies are aimed at prevention of disease progression, primarily by controlling IOP either with hypotensive topical medicines or through surgical procedures that alter outflow rates. Drugs aimed at controlling IOPs typically do one of two things: increase outflow rates, or decrease aqueous humour production. Lowering IOP to prevent disease progression has been proven to be most effective in newly-diagnosed patients, which is why early diagnosis is critical in preserving vision. Current practice aims to lower IOP to a target level that is patient-dependent, a level that is usually around 20-50% of their original IOP, with patients getting re-assessed on a regular basis to monitor disease progression (Weinreb et al., 2014).

In the event that IOP lowering drugs prove ineffective or result in inadequate IOP reduction, surgery is considered, usually aimed at the trabecular meshwork to improve drainage. A variety of options are available, primarily for POAG. Laser trabeculoplasty creates incisions at the iridocorneal angle to increase outflow, while a trabeculotomy excises parts of the meshwork (Watson et al., 1985). In patients where the blockage is too severe for the two options above, shunts or stents are implanted into the angle to create an alternate drainage pathway for easier outflow (Manasses and Au, 2016). In PACG patients, where the iris obscures the angle, iridectomies or iridotomies are performed to create incisions in the iris, or excise sections of iris, respectively (Weinreb et al., 2014).

These are all therapies aimed at IOP lowering, but the ultimate target for glaucoma treatment is neuroprotection; in some patients, RGC degeneration occurs despite reducing the IOP (Brubaker, 1996), and, as previously stated, NTG develops without IOP elevation. While IOP-lowering is indirectly neuroprotective, a considerable number of studies are attempting to develop therapies that are primarily targeted at protecting the optic nerve and the retina.

Glutamate excitotoxicity has been implicated as a pathogenic damage mechanism, and is related to activation of NMDA receptors (Sisk and Kuwabara, 1985); therefore, inhibition of NMDA-receptor activity is a therapeutic target that is being investigated. Several NMDA receptor antagonists have been evaluated for their ability to reduce glutamate toxicity; however, these compounds either had too great an affinity for NMDA receptor, resulting in neurotoxicity (Olney et al., 1991), or were very promising in pre-clinical trials but failed to provide adequate neuroprotection in clinical trials (Danesh-Meyer and Levin, 2009). Newer, more promising compounds are emerging, and await further experimentation in animal models (Fang et al., 2010).

Supply of neurotrophic factors is also a potential therapy. Retinal neurons possess receptors for a variety of trophic factors that can be exogenously supplied to improve cell health, and it is known that axonal transport malfunctions in glaucoma deprive retinal neurons from receiving vital neurotrophic support (Crish et al., 2010). Multiple factors and cytokines have also been proposed to be neuroprotective, such as basic fibroblast growth factor (Unoki and LaVail, 1994), interleukin-6 (Perígolo-Vicente et al., 2014), and erythropoietin (Bartesaghi et al., 2005), and studies are underway to test their therapeutic efficacy. One of these factors is BDNF, which has repeatedly been confirmed as a prosurvival agent for RGCs (Chen and Weber, 2001; Peinado-Ramón et al., 1996; Sawai et al., 1996; Di Polo et al., 1998). Intravitreal injections of purified BDNF in a variety of *in vivo* models of optic nerve injury have shown great promise, but the efficacy of protein treatment is short-lived and requires multiple injections (Doozandeh and Yazdani, 2016). Also, the available literature examining the effect of exogenous BDNF in models simulating glaucoma is sparse; most of the work tests BDNF in axotomy models.

Similar to BDNF, human ciliary neurotrophic factor (CNTF) has also been proven effective in protecting RGCs, both in *in vitro* RGC culture studies (Meyer-Franke et al., 1995) and in adenovirus-mediated delivery of the gene (Weise et al., 2000). A study testing viral delivery of CNTF, BDNF, or both in combination in a rat glaucoma model reported significant protection with CNTF alone. However, injections of BDNF vector alone or both CNTF and BDNF vectors did not show significant improvement. Interestingly, protein analysis of the retinas showed increased expression of CNTF in single vector injected eyes but not in eyes that were injected with both vectors (Pease et al., 2009), which may have been caused by detrimental side effects of multiple viral injections. These are challenges that must be overcome to provide a functional and sustainable therapy for glaucoma.

1.5. Apoptosis and XIAP

Another prominent focus of therapy is targeting the endpoint of the disease. Apoptosis has been well-accepted as the predominant endpoint of the mechanisms activated by glaucoma; oxidative stress, glutamate excitotoxicity, and trophic deprivation all ultimately result in cellular apoptosis. Studies looking into the mechanisms of cell death in both glaucoma patients (Kerrigan et al., 1997) and models (Garcia-Valenzuela et al, 1995; Quigley et al., 1995; Guo et al., 2005) have shown that RGCs die in a manner that resembles apoptosis, exhibiting chromatin and cytoplasm condensation, lack of an inflammatory response, blebbing, and DNA fragmentation (Kerr et al., 1972).

Apoptosis is a form of programmed cell death caused by activators of the proteolytic caspase cascade. Caspases are proenzymes that need to be cleaved for activation; the activated forms cleave critical cellular components, resulting in cell death (Cohen, 1997). Apoptosis can be initiated by intrinsic or extrinsic pathways. In the intrinsic pathway, stress signals lead to the migration of pro-apoptotic factors BAX and BAK to the mitochondria to form pores in the outer membrane (Westphal et al., 2011). Membrane permeabilization allows for the release of factors from the inner membrane space. One of these factors is cytochrome c, an electron transporter, which enters the cytosol and binds to Apaf-1 to form the apoptosome (Hill et al., 2004). This complex cleaves procaspase 9 to form the activated initiator caspase 9, triggering the caspase cascade. Caspase 9 can then target and activate caspases 3 and 7 further downstream in the pathway, eventually resulting in cell death (Cohen, 1997). The extrinsic pathway is activated by the binding of ligands to transmembrane receptors of the tumor necrosis factor (TNF) receptor (TNFR) family, which all have cytoplasmic domains called “death domains” involved in signal transmission from the cell surface to intracellular pathways (Ashkenazi and Dixit, 1998). One example of the potential signalling cascade would be the binding of the Fas ligand (FasL) to its receptor, Fas on the

cell surface, leading to the recruitment of the Fas-associated death domain protein (FADD) intracellularly. FADD combines with initiator procaspase 8 to form the death-inducing signalling complex (DISC), triggering the caspase cascade (Kischkel et al., 1995). Both intrinsic and extrinsic pathways lead to the cleavage and activation of the effector or executioner caspase 3, activating the final apoptotic pathway.

Many proteins are involved with regulating the apoptotic pathway, modulating either mitochondrial function or caspase activity. The BCL-2 class of proteins are regulators of mitochondrial function and include the abovementioned pro-apoptotic BAX and BAK. This family also includes the anti-apoptotic BCL-2 and BCL-X2, who work to prevent cytochrome c release by preserving mitochondrial membrane integrity (Westphal et al., 2011). However, these proteins can only mediate activation of the intrinsic apoptotic pathway by targeting the mitochondria. The strongest apoptotic regulators are the members of the inhibitor of apoptosis (IAP) family, which directly interact with and inhibit caspases, thereby regulating apoptosis at both the intrinsic and extrinsic pathways. There are eight members of the human IAP family, all of which contain one or more regions called the baculovirus IAP repeat (BIR) domains, zinc-binding domains consisting of 70 residues that functions as an area of protein-protein interactions (Verhagen et al., 2001). Of the IAPs, the most well-characterized and most potent apoptotic inhibitor is the X-linked inhibitor of apoptosis (XIAP). XIAP contains three BIR domains, two of which are involved with inhibiting caspases through different mechanisms (Figure 1.2). The region linking the BIR1 and BIR2 domains has been shown to inhibit effector caspases 3 and 7, while the BIR2 domain is thought to stabilise the binding (Takahashi et al., 1998; Huang et al., 2001). Isolated BIR3 domains were shown to potently inhibit initiator caspase 9 (Sun et al., 2000).

XIAP's ability to inhibit caspases can be negatively regulated by at least two known proteins:

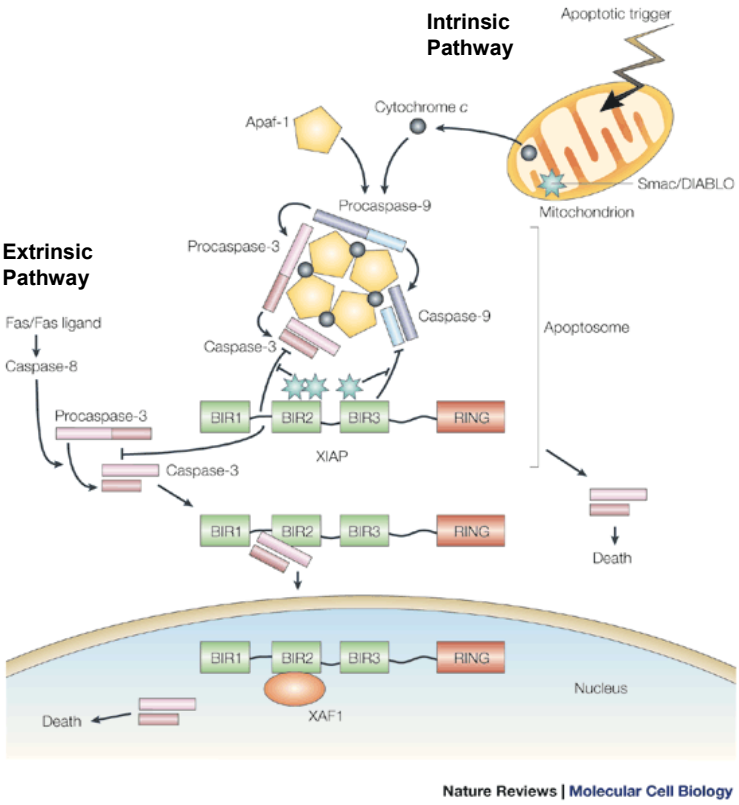

Figure 1.2. XIAP's role in inhibiting apoptosis. In extrinsic apoptosis, Fas ligand binds to its receptor, activating caspase 8, which subsequently cleaves and activates caspase 3, triggering cell death. In intrinsic apoptosis, apoptotic stimuli lead to the release of cytochrome c from the mitochondria, which binds to Apaf-1 to form the apoptosome. This complex then recruits and cleaves procaspase 9 to form the activated caspase 9, which can continue the caspase cascade by activating caspase 3. XIAP is able to bind and inhibit initiator caspase 9 via its BIR3 domain, and effector caspase 3 via its BIR2 linker region, preventing cell death initiated by both the extrinsic and intrinsic pathways. In the event that apoptosis must ensue, XIAP can be negatively regulated by two proteins: Smac/DIABLO, which is concurrently released with cytochrome c during intrinsic apoptosis and binds to the BIR2 and BIR3 domains, and XAF-1, a nuclear protein that inactivates XIAP by binding to its BIR2 domain. Figure adapted from (Holcik and Korneluk, 2001).

Smac/DIABLO, and XIAP-associated factor-1 (XAF-1). Smac/DIABLO is an IAP antagonist that is released from the mitochondria alongside cytochrome c during intrinsic apoptosis, and inhibits XIAP by binding to its BIR2 and BIR3 domains, disrupting the formation of XIAP-caspase complexes via steric hindrance and competitive binding, respectively, and allowing the continuation of the caspase cascade (Chai et al., 2000; Liu et al., 2000). XAF-1 is a zinc-finger protein that is able to bind XIAP and suppress its caspase inhibition activity. It resides in the nucleus and can effect the translocalization of cytosolic XIAP to the nucleus to neutralize XIAP (Liston et al., 2001). Unlike Smac/DIABLO, XAF-1 constitutively interacts with cellular XIAP and does not require an activating signal.

Aside from its BIR domains, XIAP also contains a 'really interesting new gene' (RING) domain, which functions as an E3 ubiquitin ligase alongside XIAP's ubiquitin-associated domain (UBA) to catalyze autoubiquitination of XIAP for proteosomal degradation in the event that apoptosis must continue (Galbán and Duckett, 2010). This domain can also function to ubiquitinate other proteins, including other members of the IAP group (Yang et al., 2000), caspases (Suzuki et al., 2001), and its inhibitor, Smac/DIABLO (MacFarlane et al., 2002). Although it is known that XIAP is involved in these pathways, the activation and regulation of its ubiquitin signalling as well as the number of signalling pathways XIAP is involved in is still unknown.

XIAP has also been implicated in several other pathways, mostly owing to the IAP family's modular structure. While XIAP's BIR2 and BIR3 domains were known to bind caspases, the function of XIAP's BIR1 domain was largely unknown for several years. Lu et al. (2007) discovered that XIAP's BIR1 domain forms a complex with transforming growth factor β-activated kinase 1 (TAK1) binding protein (TAB1), which subsequently activates TAK1 (Lu et al., 2007). BIR1 acts in combination with XIAP's RING domain to activate TAK1, which mediates activation of the nuclear factor kappa B (NF-κB)

pathway and plays an important role in inflammation (Ajibade et al., 2013). Interestingly, XIAP has been implicated in mediating canonical and non-canonical NF-κB signalling pathways, but it has also been shown that NF-κB activates expression of XIAP, resulting in a feedback loop of pro-survival signalling (Stehlik et al., 1998).

Many studies have shown that XIAP is heavily involved in regulating immunity and inflammation, although the mechanisms are unclear. Bacterial infections in XIAP knockout mice failed to kick-start an immune response (Pedersen et al., 2014), while loss-of-function mutations in XIAP are associated with the development of hyperinflammation, hypothesized to be caused by uncontrolled cytokine production (Damgaard et al., 2013). XIAP has also been shown to inhibit necroptosis and pyroptosis, both types of programmed inflammatory cell death. XIAP inhibits receptor-interacting serine/threonine-protein kinase 3 (RIPK3), which activates cytokine production and leads to necroptosis (Wong et al., 2014). RIPK3 can also induce TNF-α secretion, which is a ligand in the extrinsic apoptotic pathway (Wong et al., 2014). Furthermore, XIAP has been shown to prevent formation of the inflammasome which is known to activate pyroptosis (Yabal et al., 2014), thereby protecting against a variety of forms of cell death.

1.6 Animal Models of Glaucoma

Animal model development for glaucoma has been a difficult process, owing to the multifactorial nature of the disease. Most models of glaucoma are the result of induced ocular hypertension, which does not entirely assimilate the complexities of the disease presentation. However, these models have greatly expanded our understanding of the progression and development of the disease thus far, though there are still efforts to establish better, more robust models.

A variety of animals of different sizes have been used to develop glaucoma models, including primates, cats, dogs, and rodents. Each animal has its own advantages and disadvantages to being chosen. Primates are almost identical to humans in terms of ocular physiology and anatomy, and make for excellent models when analyzing the variations of retinal or optic nerve structure in response to the disease. However, they are expensive, limited in availability, and difficult to handle. On the opposite side of the spectrum, rodent models, especially rats, are the most developed and used for studies in glaucoma. Although not as similar to humans in ocular structure or function as primates, rodents are much easier to manipulate experimentally.

One of the most well-characterized models of glaucoma is the highly inbred DBA2/J mouse strain. These mice have mutations in two genes, *Tyrp1* and *Gpnmb*, encoding for tyrosinase-related protein 1 and glycosylated transmembrane protein, respectively (Anderson et al., 2001). The combined interactions result in the development of iris stromal atrophies and iris pigment dispersions; the iris undergoes severe depigmentation and deterioration, and the debris enters and clogs the trabecular meshwork, leading to IOP elevation (Anderson et al., 2001). This pigmentary glaucoma is similar to POAG in humans, as the disease results in a gradual increase in IOP starting at 6 months of age, which leads to severe damage phenotypes around 12 months of age (Libby et al., 2005).

While the pigmentary model is very true to the development of POAG, the course of glaucoma development is not conducive to short-term studies, and the neurodegeneration varies greatly from animal to animal, because there is no way to manipulate disease development. Glaucoma models of inducible ocular hypertension were developed to reduce variability and the time of disease onset. Methods for IOP elevation can differ depending on the tools available and the animal used, but are primarily aimed at restricting humour outflow at either the trabecular meshwork or the episcleral veins. One of the first

models to be developed is the saline injection model. Hypertonic saline is injected into the episcleral veins of rats to induce sclerosis and slow aqueous humour outflow. The technique results in moderate IOP elevation, which in some cases can be sustained for up to 200 days, causing significant damage to the retina and optic nerve (Morrison et al., 1997). However, development of the model takes years to perfect and requires immense surgical precision. There is also a considerable amount of variability in the level of IOP increase, and some studies have reported that repeat saline injections were required when initial treatment failed (Fortune et al., 2004). The technical challenges faced with using this model and its inconsistent IOP elevation stressed the need for a simpler and less variable model system, leading to the development of the microbeads model. Injections of polystyrene or magnetic microbeads into the anterior chambers of rodents successfully managed to induce consistent and sustained IOP elevation. The beads settled against the iridocorneal angle, obstructing drainage of the humour (Sappington et al., 2010). While earlier adaptations required multiple injections, newer versions were able to maintain the IOP increase without requiring further manipulations, and resulted in very little inter-animal variability. We have chosen to test our therapy in this model.

1.7 Electrophysiology in Mice

Electroretinography (ERG) is a valuable tool to measure the function of retinal cells non-invasively. It measures the electrical activity of the cells generated in response to light stimulus through the placement of electrodes on the surface of the cornea; the corneal electrodes are grounded by the insertion of needle electrodes in the tail and the head of mice. The generated waveforms are a sum of the electrical impulses from the retinal neurons in response to flashes of light at different intensities, and measure both amplitude and latency of the responses. ERGs were primarily designed for patient testing

but have been adapted for use in a wide variety of animals, including rodents. The work described in this thesis used two types of ERG tests to assess murine retinal function: the full-field scotopic flash ERG and the pattern ERG (PERG).

The full-field ERG is a summation of the electrical responses from a variety of retinal neurons and glial cells. It is composed of multiple components, each one tracing back to a specific retinal cell type. The first component is a negative a-wave, caused by hyperpolarization of the photoreceptor cells, the rods and the cones (Clark and Kraft, 2012). This drop is followed by the depolarization of their synaptic partners, the ON bipolar cells, which creates a trans-retinal current and subsequently depolarizes the Müller glia as well, resulting in the b-wave (Clark and Kraft, 2012). The ascending b-wave contains a series of wavelets called the oscillatory potentials, which are generated by amacrine cells. The parameters of the test (background, stimulus intensity, wavelength) can be manipulated to isolate specific cell types and compare function (rod-driven vs cone-driven) (Weymouth and Vingrys, 2008).

While the full-field is able to provide information on most of the retinal cells, it is unable to isolate the response of the RGCs, which are the cells of primary focus in glaucoma. To assess RGC function, the PERG test is used. The PERG is a variation of the ERG, consisting of alternating black and white bars or checkerboards displayed at a specific frequency. This pattern reversal generates adjacent out-of-phase ERG elements which sum and cancel each other out. In contrast, RGC responses are in-phase and additive, and sum to generate a waveform, resulting in the PERG (Porciatti, 2007). The trace is composed of three components: a negative N35, a positive P50, and a negative N95. The names of the peaks are derived from the mean vertex latencies; the N and P denote whether the component will be negative or positive. The peak-to-peak component between the N35 and the P50 is the P50 amplitude, which is a measure of RGC somal function, while the component between the P50 and the N95 is the N95

amplitude, indicative of RGC axon function (Holder, 2001). In mice, the N35, P50, and N95 components are termed the N1, P1, and N2, respectively.

While electroretinography is able to provide sensitive information regarding retinal cell health, the effects of glaucoma extend beyond the retina and affect the majority of the visual pathway. In addition to the ERG tests, visual evoked potentials (VEP) were also employed to gain a complete understanding of the extent of the damage in the disease model. VEPs are widely used in the diagnosis and assessment of a variety of optic neuropathies; increased demyelination can result in longer latencies, while axon loss can affect VEP amplitude and waveform structure (Walsh et al., 2005). Light stimuli are introduced to the eye via corneal electrodes, but, unlike in electroretinography, the responses are measured at the brain via a subdermal electrode inserted to rest above the visual cortex. VEPs are composed of three components: a positive C1, a negative P1, and a positive N1, which correspond to the P1, N1, and P2 in mice. Each component is the response derived from different retinal areas (Baseler and Sutter, 1997), which map to different locations in the cortex (Russo et al., 2001).

Each of these three tests provide valuable information regarding the health of the components of the visual pathway. Used in combination, they can assess the signalling integrity from the retina to the brain, providing a complete measure of retinal and optic nerve function.

1.8 Rationale and Hypothesis

Glaucoma is a progressive neurodegenerative disease that develops asymptomatically and affects millions worldwide. Current treatments are aimed at lowering IOP, the most predominant risk factor, but IOP-independent forms of the disease are known to develop, and reducing pressure is not always effective. Multiple factors contribute to the pathology of glaucoma, but all forms of the disease ultimately end in the death of retinal ganglion cells and their axons, primarily via apoptosis. Of the several compounds that are known to inhibit apoptosis, XIAP is the most potent, and is a proven neuroprotective agent, both structurally and functionally. We propose that overexpression of XIAP in the retina will be effective in preserving vision in a model of glaucoma.

2.0 MATERIALS AND METHODS

2.1 Animals

Adult C57BL/6J mice (n=48; 24 males, 24 females; 2 months old) were purchased from Jackson Laboratories (Bar Harbor, Maine) and housed under standard light/dark protocols throughout the experiment. All procedures adhered to the Association for Research in Vision and Ophthalmology (ARVO) statement for the Use of Animals in Ophthalmic and Vision Research, and the guidelines set by the University of Ottawa Animal Care and Veterinary Service.

2.2 Viral Vector Constructs

Adeno-associated virus type 2 serotype 2 (AAV2/2) vectors were generated and obtained from William Hauswirth (University of Florida). AAV2-XIAP encoded human XIAP in the open reading frame with an N-terminal hemagglutinin (HA) tag, while its injection control vector, AAV2-GFP, encoded GFP. Gene expression in both vectors was regulated with a cytomegalovirus (CMV) enhancer and a chicken beta actin (CBA) promoter, and enhanced with a woodchuck hepatitis virus posttranscriptional regulatory element (WPRE). Constructs were generated, purified, and titered as previously described (Hauswirth et al., 2000, Zolotukhin et al., 2002).

2.3 Animal Preparation for Injections and Surgeries

All surgeries were performed on animals anesthetized with 2% isoflurane gas. Surgery eyes were dilated with 1% tropicamide (Mydriacyl), locally anesthetized with 0.5% proparacaine hydrochloride (Alcaine), and hydrated with 0.3% hypromellose (Genteal). Contralateral eyes were treated with only Genteal to prevent corneal drying. Injected eyes were treated with an ophthalmic antibiotic (B.N.P.;

bacitracin, neomycin, polymyxin B) and animals received an injection of buprenorphine (0.04 mg/kg) for pain management immediately following surgery and 24 hours after surgery.

2.3a. Viral Vector Injections

Viral vectors were injected intravitreally one week following baseline *in vivo* ERG and IOP measurements. Immediately prior to viral injections, a 20-gauge V-lance knife was used to create an incision in the sclera just below the limbus, taking care to avoid contact with the lens. The virus was then injected through the preformed opening into the vitreous using a Hamilton syringe attached to a blunt 30-gauge needle. Animals received 1 µL of $1x10^{12}$ viral genomes (vg)/mL of either AAV2-XIAP (n=24) or AAV2-GFP (n=24) in their left eyes only. The injected solution was a combination of virus and fluorescein tracer (50:1) in order to visualize the virus in the vitreous.

2.3b. Microbead Injections for Development of Glaucoma Model

Intracameral injections to induce IOP elevation were performed three weeks following intravitreal injections of virus. A solution of magnetic microbeads (Dynabeads M-450 Epoxy; Life Technologies) or BSS (control) was injected intracamerally into the left eyes of the animals as previously reported (Ito et al., 2016). Intracameral injections were performed with pulled glass capillary needles (World Precision Instruments), which were bevelled according to the specifications of the developers of the model (Ito *et al.*, 2016). Needles were attached to a Hamilton syringe and used to pull up 1.5 µL of beads solution at a concentration of $1.6x10^{6}$ or BSS as the control. The needle was used to puncture the cornea near the limbus at a 45° angle and the beads or BSS were injected into the anterior chamber. A handheld magnet (0.45 Tesla) was used to evenly distribute the beads around the iridocorneal angle, and the mice were laid on their side on a heating pad to recover with the injected eye facing upwards. Animals

from both groups that received AAV2-XIAP or AAV2-GFP were split evenly to receive beads or BSS, resulting in four groups of twelve animals with a 1:1 ratio of males to females that were injected with a combination of AAV2-XIAP or AAV2-GFP and microbeads (glaucomatous) or BSS (control). Following glaucoma induction, retinal health and function were monitored for a period of six weeks using a series of *in vivo* tests (see below).

2.4 Anesthesia for IOPs, Fundus Imaging, and Electroretinography Measurements

Prior to any *in vivo* measurements, all animals received intraperitoneal injections of 50mg/kg ketamine and 1mg/kg medetomidine. Following the procedures, the anesthetic was reversed using 1mg/kg atipamezole hydrochloride, and each animal received 1-2 mL of saline subcutaneously to prevent dehydration and was left to recover on a heating pad.

2.5 IOP Measurements & Fundus Imaging

IOPs were measured with a Tono-Pen VET (Reichert, Inc.). The device was used without a cover and was gently placed on corneas of the animals at a perpendicular angle to the cornea. The Tono-Pen automatically calculates a mean of four independent readings, and each mean was considered one measurement. A total of five measurements were averaged to give the mean IOP recorded for each eye. IOPs were always taken between 10 am and 12 pm in anesthetized mice and each mouse was measured at five different timepoints: baseline, and 1, 2, 3, and 6 weeks after beads injections. Fundus images were acquired following IOP measurements using a Phoenix Micron III Retinal Imaging Microscope (Phoenix Research Laboratories, Inc.).

2.6 Electroretinography (ERGs) and Visual Evoked Potentials (VEPs)

Retinal function was assessed using the Celeris system (Diagnosys, Inc.) paired with the Espion software (Diagnosys, Inc.). Animals were dark-adapted overnight, anesthetized under red light (660 nm), and placed on a heated (37°C) platform to maintain body temperature. Eyes were dilated with 1% tropicamide (Mydriacyl), locally anesthetized with 0.5% proparacaine hydrochloride (Alcaine), and hydrated with 0.3% hypromellose (Genteal). Ag/AgCl corneal electrodes were placed on either eye, with a looped electrode placed in the mouth as the reference and a needle electrode inserted in the tail as the ground. The animals underwent a total of three different tests:

2.6a. Full Field ERG

Animals were subjected to a white flash stimulus via the corneal electrodes and a total of three traces were recorded for each eye. The flash stimulus was presented at a frequency of 1 Hz and an intensity of 0.01 cd.s/m^2. Oscillatory potentials were acquired at an intensity of 3 cd.s/m^2. Data acquisition was conducted at a frequency of 2000 Hz for a sweep duration of 10 ms pre-stimulus to 300 ms post-stimulus.

2.6b. Simultaneous Flash ERG & VEP

A needle electrode was inserted below the scalp to rest against the visual cortex, and animals were subjected to a white flash stimulus via the corneal electrodes. A total of 100 traces were recorded for each eye. The flash stimulus was presented at a frequency of 1 Hz and an intensity of 0.05 cd.s/m^2. Data acquisition was conducted at a frequency of 2000 Hz for a sweep duration of 10 ms pre-stimulus to 300 ms post-stimulus.

2.6c. Pattern ERG (PERG)

The stimulated eye was presented with a monitor viewed through a corneal electrode, with a Ag/AgCl flash corneal electrode placed on the contralateral eye. The monitor displayed alternating horizontal black and white bars at 100% contrast, and an intensity of 50 cd.s/m^2, a spatial frequency of 0.155 cycles/degree, and a temporal frequency of 1 Hz. The bars were viewed at a distance of 1100 mm. A total of 200 traces were generated. Data was acquired at a frequency of 1000 Hz, from 50 ms pre-trigger to 420 ms post-trigger. Final waveforms were scored by eliminating any traces above +30 μV or below -30 μV.

2.7 Optic Nerve Preparation and Processing

Mice were anesthetized using dry ice and transcardially perfused with 8-10 mL of 4% PFA. The skull was bisected to expose the brain which was removed to visualize the optic nerves. The nerves were cut at the intersection point between nerve and globe of the eye at one end, and approximately 2 mm below the optic chiasm at the other end, where they were pinched to distinguish between both ends. The left and right nerves were separated at the chiasm and fixed individually in Karnovsky's fixative (4% PFA, 2% glutaraldehyde, 0.1M sodium cacodylate in PBS, pH 7.4) overnight. The eyes were enucleated and processed separately following removal of the nerves (see Section 2.10 below).

The optic nerves were post-fixed the following day in 2% osmium tetroxide in distilled water for 2 hours, and washed twice for 5 minutes with distilled water. The segments were then dehydrated in ascending concentrations of alcohol for an hour each, then transferred into 50/50 Spurr's resin/acetone for 1 hour, then into pure resin overnight. Spurr's resin was changed the next day, and the nerves were embedded in fresh resin and polymerized in moulds overnight at 70°C.

2.8 Optic Nerve Analysis with Light Microscopy

Optic nerve cross-sections were produced using a Leica Ultracut R Ultramicrotome. Sections were cut to 0.5 μm, mounted onto glass slides, and stained with 1% toluidine blue. Sections were examined using light microscopy under a Zeiss Axioplan microscope equipped with an Axiocam Hrc camera to analyze axons. ImageJ software was used to calculate optic nerve diameter, area, and axon numbers. For axon counts, five square grids of 1300 μm^2 were overlaid on each optic nerve in a cross pattern, and the number of axons within each square was counted (Figure 2.1). The average of the counts from the five areas gave the mean count for the number of axons per square in that optic nerve.

2.9 Optic Nerve Analysis with Transmission Electron Microscopy

90nm thin sections for TEM were mounted onto copper grids and stained on a droplet of UranyLess (a commercial preparation of Lanthanides) followed by lead citrate. The grids were then screened and digital images were captured using a Hitachi H-7100 Transmission Electron Microscope.

2.10 Processing of Retinas

Eyes were enucleated and processed for sectioning. A 25-gauge needle was used to puncture the eye and fine scissors were used to cut along the limbus to remove the cornea and lens. The eyecups were fixed in 4% PFA for 15 minutes, then rinsed twice in PBS and washed for an hour in PBS. Specimens were transferred to 30% sucrose at 4°C overnight, then incubated in 50/50 sucrose/OCT mix overnight at 4°C. Eye cups were frozen in trays filled with 50/50 sucrose/OCT with the limbus against the tray and stored at -80°C until sectioning. Samples were sectioned at 10 μm along the sagittal plane onto Fisherfrost™ Superfrost™ slides and air-dried for 2 hours before storing at -20°C.

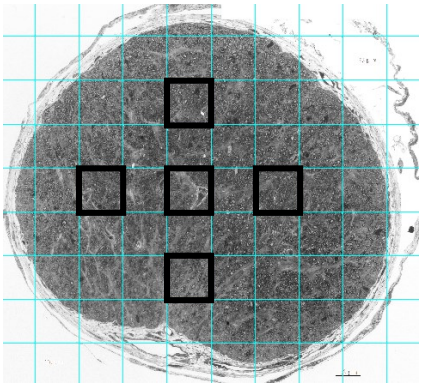

Figure 2.1: Schematic of cross pattern on grid for axon counts. Each square has an area of 1300 μm^2. Axon counts were conducted for each of the five squares outlined in black and averaged to calculate the mean for each optic nerve.

2.11 Histological Analysis

Immunostaining was performed on cryosections and flatmounts. Sections were post-fixed for 3 minutes in 4% PFA, washed 3x in PBS, and blocked for 1 hour in a solution of 10% goat serum, 1% BSA, and 0.5% Triton X-100 in PBS. Slides were then incubated overnight in a primary antibody solution of 3% goat serum and 0.5% Triton X-100 in PBS. The following day, slides were washed 3x in PBS and incubated for 1 hour in secondary antibody solution with 3% goat serum and 0.5% Triton X-100 in PBS. Slides were then washed in PBS, counterstained with DAPI, and mounted with antifade reagent (1% N-propyl gallate in 50/50 glycerol/PBS). For flatmounts, retinas were isolated from enucleated eyes and attached to nitrocellulose membranes with the GCL layer facing upwards before fixing in 4% PFA for 30 minutes. Retinas were washed 2x in 0.5% Triton X-100 in PBS, then carefully detached from the membranes and treated to ascending concentrations of sucrose for 10 minutes each at 4°C, followed by a freeze/thaw cycle (-80°C/RT). The specimens were incubated in a primary antibody solution with 2% goat serum and 2% Triton X-100 in PBS for at least two nights. Retinas were washed twice in PBS, then incubated in secondary antibody solution with 2% goat serum and 2% Triton X-100 in PBS for 2 hours, followed by two PBS washes including a DAPI counterstain. Specimens were mounted onto slides using antifade and coverslipped. Immunostaining was performed using the following primary antibodies: mouse anti-HA (1:100; Sigma-Aldrich, Inc.), rabbit anti-RBPMS (1:50; PhosphoSolutions, Inc.), rabbit anti-Pax6 (1:500; BioLegend, Inc.), and rabbit anti-caspase 3 (1:50; Abcam, Plc.). Secondary antibodies used were mouse and rabbit Cy3 at 1:500 (Jackson ImmunoResearch, Inc.). Sections were examined at 200x magnification using a Zeiss Axio Imager microscope.

3.0 RESULTS

We decided to test the neuroprotective abilities of AAV2-XIAP in a previously established mouse model of ocular hypertension developed by Ito et al. (2016). Preliminary experiments were performed to ensure the model could be reproduced in our lab, and to perfect the technical aspects of the surgeries in order to minimize variability in our IOP recordings, and reduce damage to the corneas and lenses. Once the procedure was optimized, we conducted the definitive set of experiments to determine the effects of XIAP overexpression. Baseline IOP and functional measurements were obtained before any injections to ensure all test subjects were healthy. Any animals showing signs of corneal/lens defects or reduced visual responses were eliminated (n=2). Animals included in the study were given an intravitreal dose of 1 μL of $1x10^{12}$ vg/mL of AAV2-XIAP or AAV2-GFP in their left eyes only. Three weeks later, ocular hypertension was induced in the left eyes by injecting magnetic microbeads into the anterior chamber and using a handheld magnet to settle the beads into the iridocorneal angle. BSS was injected as a control. Animals were followed for six weeks following microbead injections. Fundus imaging performed two weeks after the intravitreal viral injections showed robust GFP expression in animals that received AAV2-GFP (Figure 3.1a). Immunostaining the retina for the HA-tag (found in the XIAP construct) at six weeks following beads surgeries confirmed the presence of XIAP in the ganglion cell layer and optic nerve of animals that received AAV2-XIAP (Figure 3.1c,d).

3.1 Beads injections were able to elevate and sustain pressure increase

IOP measurements were a crucial component in ensuring the injections were elevating IOP, and were taken in anesthetized mice at six different timepoints: baseline, and 1, 2, 3, 4, and 6 weeks after beads surgeries. Similar to the findings of the model developers, we noticed a significant and sustained elevation of IOP (Figure 3.2). At one week-post beads injections, IOP was increased by 35% in XIAP-injected

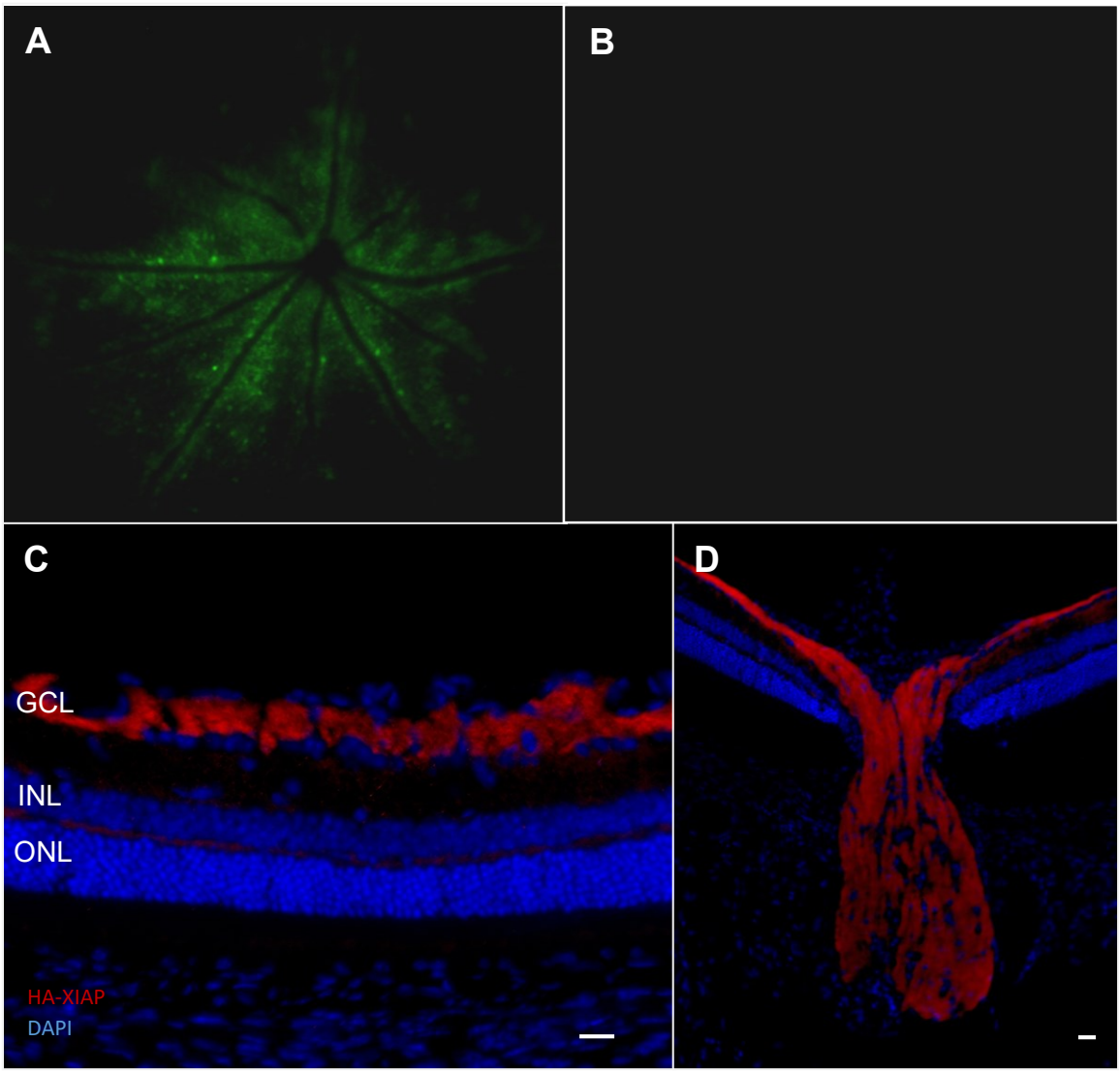

Figure 3.1. Expression of GFP and HA-tagged XIAP in retinas following intravitreal injections. a) Fluorescent fundus image of the retina two weeks following an intravitreal injection of AAV2-GFP shows good viral coverage and strong protein expression while **b)** the contralateral uninjected eye shows no fluorescence. **(c,d)** Immunostaining for the HA-tag in retinas sampled nine weeks after AAV2-XIAP injections show robust expression of XIAP in the **c)** ganglion cell layer (GCL) and **d)** optic nerve. Scale bars: 20 μm.

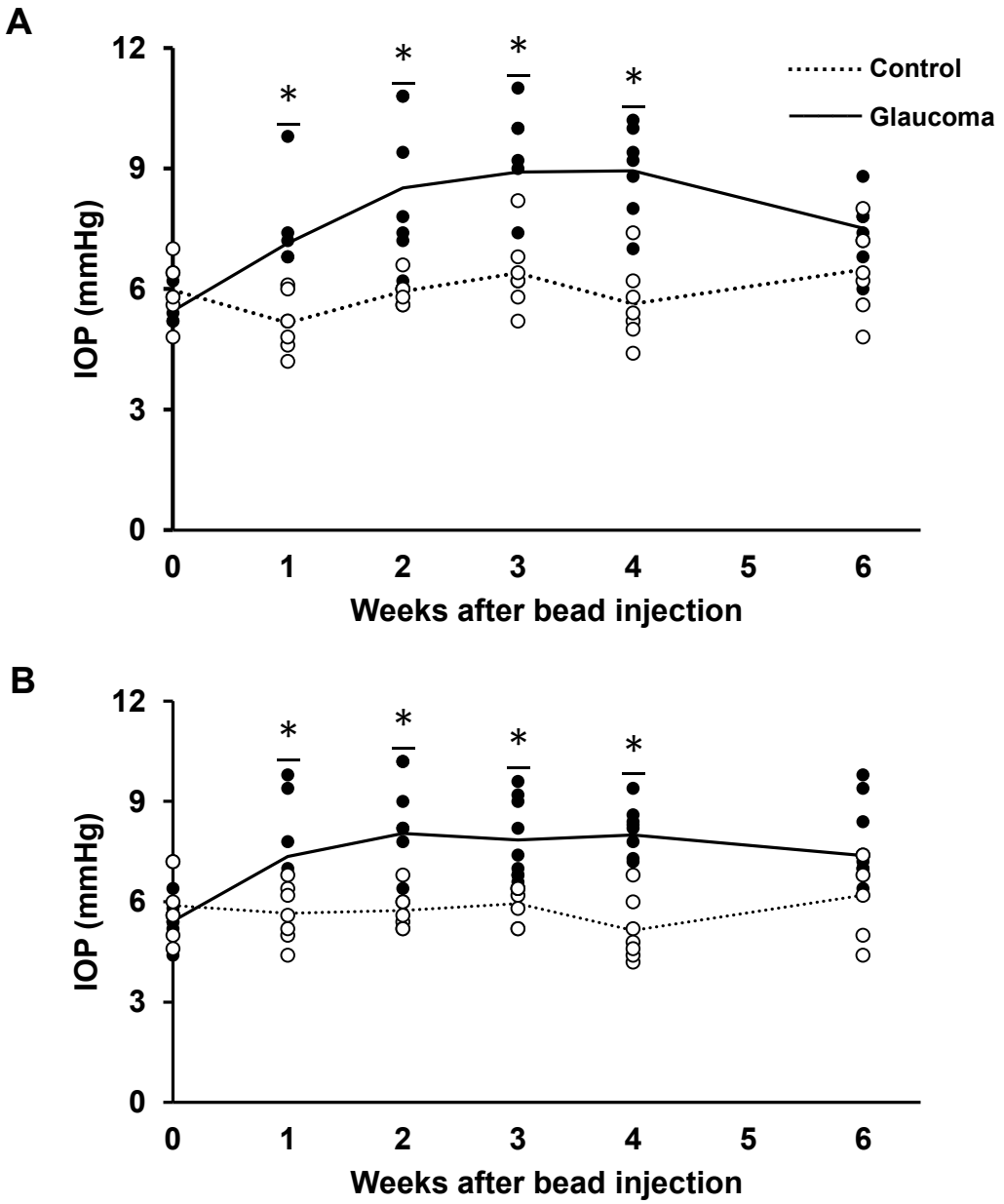

Figure 3.2. Glaucoma surgeries successfully elevate pressure and sustain increase for four weeks. Mean IOP shown for **a)** GFP- and **b)** XIAP-injected animals, taken in anesthetized mice using a Tono-Pen. Each marker represents the mean of five measurements taken for one animal. Student's T-test, *$p<0.05$. GFP control: n=7; XIAP control: n=6; GFP glaucoma: n=7; XIAP glaucoma: n=9.

animals and 29% in GFP-injected animals. IOP remained elevated at an average of 8±1.1 mmHg (mean ±SD) in XIAP-injected glaucomatous eyes and 8.5±1.1 mmHg in GFP-injected glaucomatous eyes for up to four weeks, a rise from baselines of 5.4±0.4 mmHg and 5.5±0.5 mmHg respectively. In contrast, BSS-injected controls maintained a consistent average of 5.8±0.7 mmHg in GFP-injected eyes and 5.9±0.8 mmHg in XIAP-injected eyes until six weeks. These IOP elevations were significantly different ($p<0.05$) from controls at 1, 2, 3, and 4 weeks following glaucoma induction.

3.2 XIAP prevents functional impairment in RGCs

Visual function was assessed using a series of *in vivo* tests, all measuring activity at different points in the visual pathway. The dark-adapted flash ERG protocol was used to evaluate photoreceptor, interneuron, and amacrine cell responses, in order to test if the model affected cells beyond the ganglion cell layer. The resulting waveforms have three components: the a-wave (measure of photoreceptor function), the oscillatory potentials (measure of amacrine cell function) and the b-wave (measure of interneuron function). Analysis of the results of the test showed that none of the three cell types assessed were affected by the IOP elevation. Neither a-waves nor b-waves were significantly different between the glaucomatous or control groups at six weeks following glaucoma induction, suggesting that the IOP elevation is not affecting the inner or outer nuclear layers (Figure 3.3). Oscillatory potentials were also not significantly different at both timepoints between the GFP and XIAP glaucoma groups or between the two control groups (Figure 3.4). These results all suggest that the IOP elevation does not affect any of the retinal cells beyond the ganglion cell layer.

RGC responses were recorded with a pattern ERG (PERG) stimulator, which is the tool predominantly used in the field. The stimulator presents an alternating pattern of black and white horizontal bars on a screen viewed through a corneal electrode by the animal in order to derive a trace

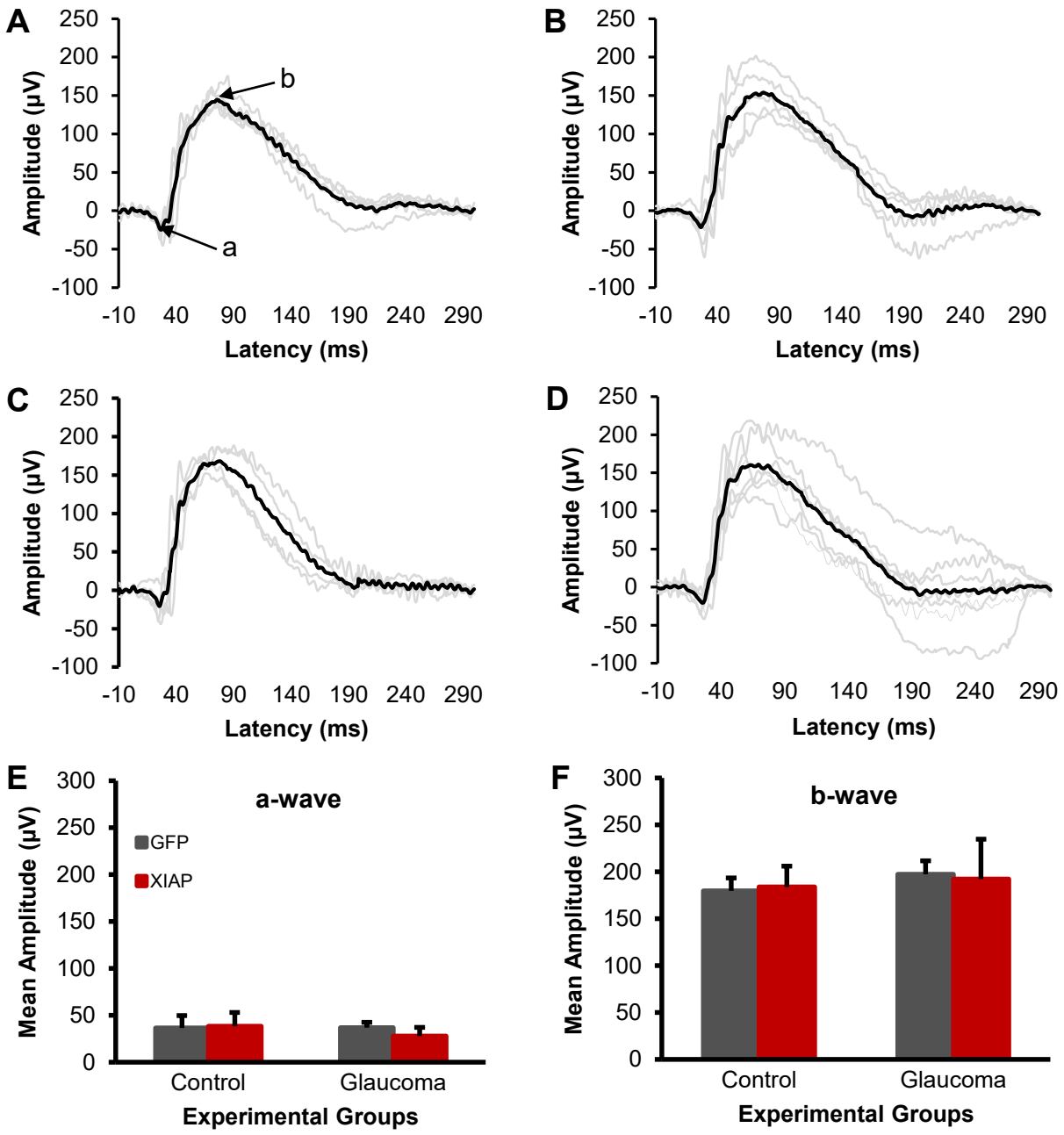

Figure 3.3. Photoreceptors and interneurons remain intact. **(a-d)** Average and individual waveforms from the dark-adapted rodent ERG tests for **a)** GFP control, **b)** XIAP control, **c)** GFP glaucoma, and **d)** XIAP glaucoma animals. Each test subject's individual waveform (average of three traces total) is shown in grey, with the average of the individual waveforms shown in black. Results shown are from tests taken at six weeks after glaucoma induction. **(e-f)** Mean amplitudes of **e)** a-waves and **f)** b-waves show no significant differences between glaucoma or control groups. GFP control: n=5; XIAP control: n=5; GFP glaucoma: n=4; XIAP glaucoma: n=7. Error bars = standard deviation.

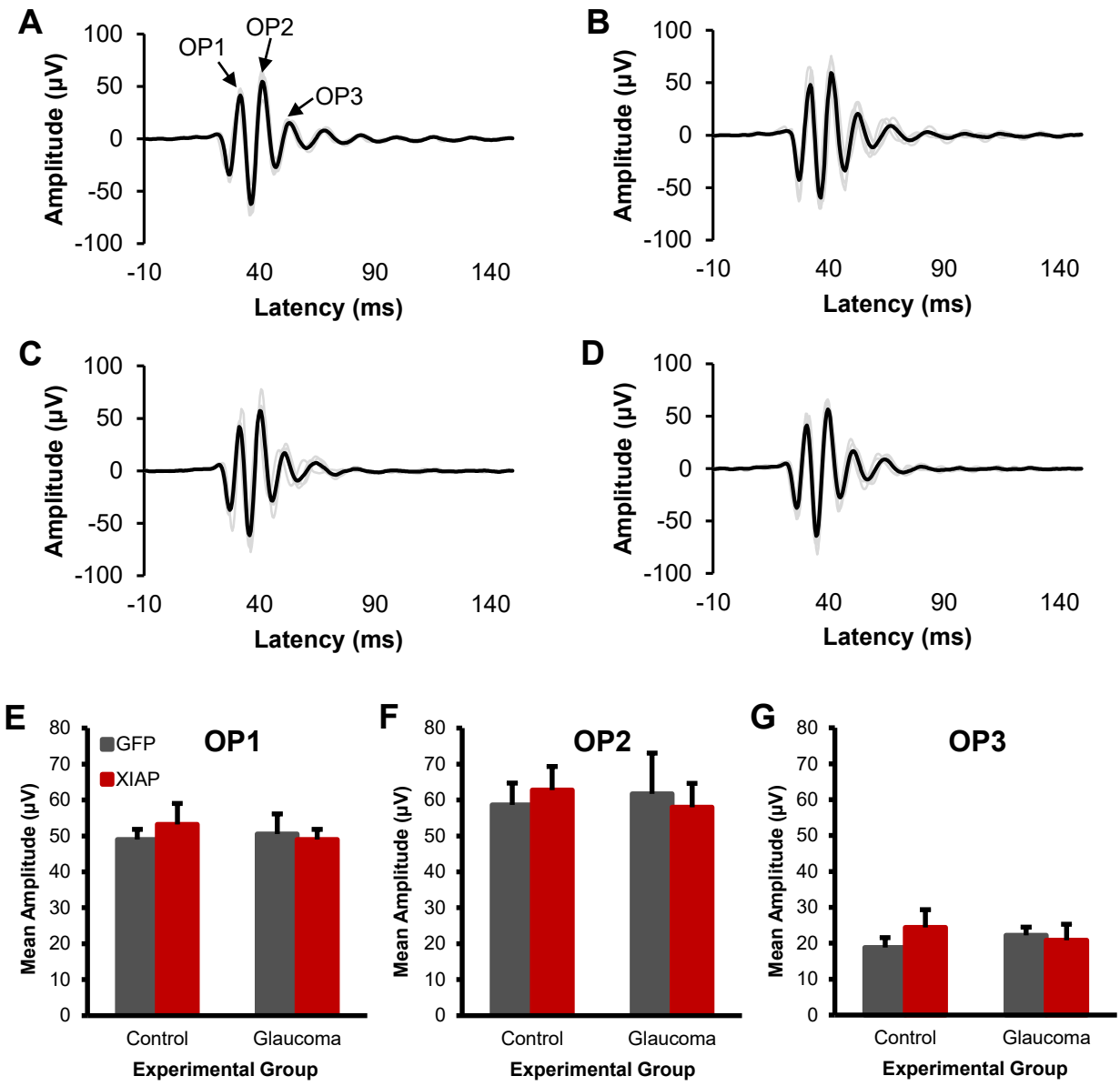

Figure 3.4. Amacrine cells remain intact. **(a-d)** Average and individual waveforms of the oscillatory potentials (OPs) for **a)** GFP control, **b)** XIAP control, **c)** GFP glaucoma, and **d)** XIAP glaucoma animals. Each test subject's individual waveform (average of 100 traces total) is shown in grey, with the average of the individual waveforms shown in black. **(e-g)** Mean amplitudes of **e)** OP1, **f)** OP2, and **g)** OP3 show no significant differences between glaucoma or control groups. Error bars = standard deviation.

that is comprised of two components, the P1 and N1, which correspond to ganglion cell soma and axon function, respectively. Analysis of the PERG traces at six weeks showed that there were no differences between the XIAP- or GFP-injected control groups that received BSS (Figure 3.5). XIAP glaucoma animals were also not different from their BSS controls and displayed waveforms with similar amplitudes. However, GFP glaucomatous eyes showed significantly impaired RGC responses in comparison to the XIAP glaucomatous eyes. At six weeks, both P1 and N1 components were reduced in the GFP glaucoma traces, with a 43% reduction in P1 and a 32% reduction in N1 compared to XIAP glaucoma eyes, suggesting that XIAP was able to protect the ganglion cell bodies and axons from functional loss triggered by elevated IOPs. It was also necessary to evaluate the integrity of signalling from the retina through the optic nerve into the visual cortex. We used a flash visual evoked potential (VEP) test to measure the strength of the potentials passed to the visual cortex by inserting a subdermal needle electrode in the scalp to rest against the skull. We expected to see reductions in signalling in the GFP glaucoma animals with this test because of the amplitude reduction witnessed in the PERG. However, the VEP showed there were no significant differences between the two glaucoma groups (Figure 3.6). In fact, we noticed that although the waveforms generated were well-defined, there was a high degree of inter-animal variability in the traces, particularly in the amplitude, which may have impacted the statistical analysis and prevented the results from reaching significance.

Overall, functional analysis showed that the pressure elevation in the model did not damage retinal cells in the inner or outer nuclear layer, but did impair signalling in the ganglion cells starting at three weeks, which remained significant until six weeks. Overexpression of XIAP prevented that loss in the glaucoma model, suggesting that XIAP is able to protect against RGC dysfunction.

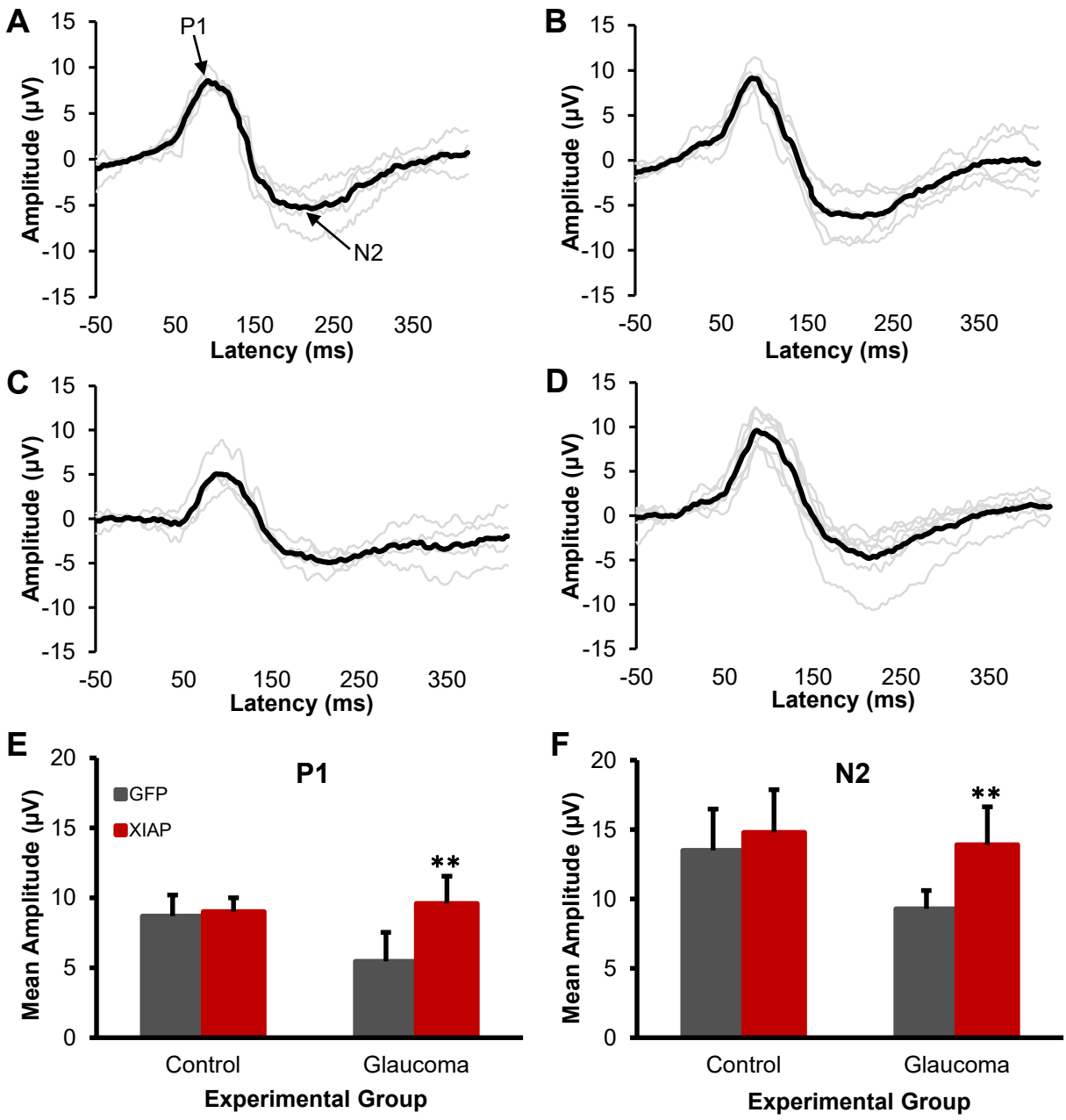

Figure 3.5. XIAP protects against RGC dysfunction in a glaucoma model. (a-d) Average and individual waveforms from the pattern electroretinography (PERG) tests for **a)** GFP control, **b)** XIAP control, **c)** GFP glaucoma, and **d)** XIAP glaucoma animals. Each test subject's individual waveform (average of 200 traces total) is shown in grey, with the average of the individual waveforms shown in black. **(e-f)** Mean amplitudes of **e)** P1, and **f)** N2 are significantly improved in XIAP glaucoma animals compared to GFP glaucoma animals. Student's T-test, **p<0.01. Error bars = standard deviation.

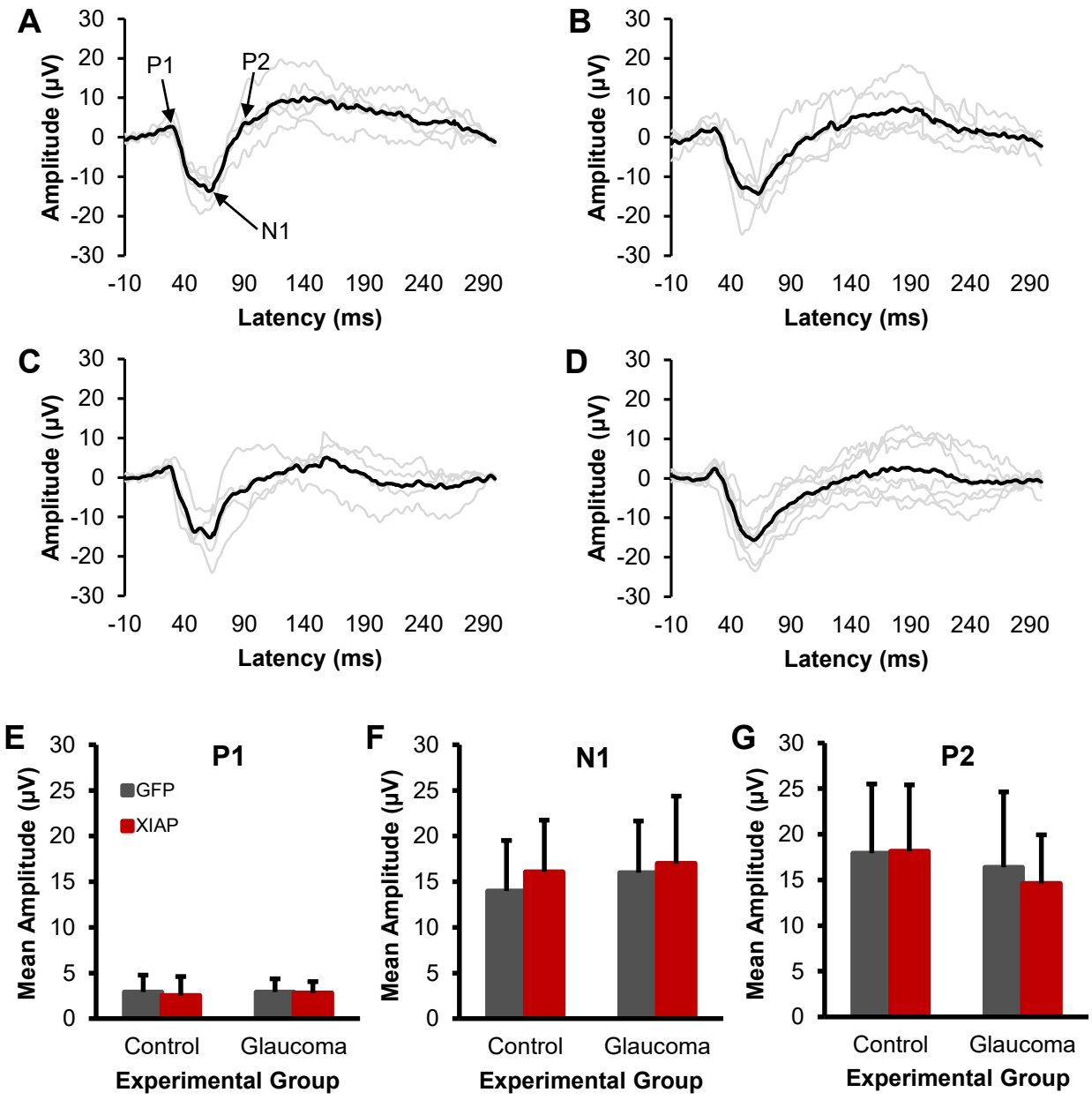

Figure 3.6. Signalling to the visual cortex remains intact. **(a-d)** Average and individual waveforms from the visual evoked potential (VEP) tests for **a)** GFP control, **b)** XIAP control, **c)** GFP glaucoma, and **d)** XIAP glaucoma animals. Each test subject's individual waveform (average of 100 traces total) is shown in grey, with the average of the individual waveforms shown in black. **(e-g)** Mean amplitudes of **e)** P1, **f)** N1, and **g)** P2 show no significant differences between glaucoma or control groups. Error bars = standard deviation.

3.3 XIAP protects RNFL from degeneration

After six weeks of monitoring disease progression, retinas and optic nerves were sampled for histology. Retinas were sectioned and stained with RBPMS, a marker for RGCs, and hematoxylin and eosin (H&E), to see if the structural data mirrors the evidence for XIAP neuroprotection we saw with the functional data. We immunostained retinas with RBPMS and performed ganglion cell counts, which did not show any significant differences in RGC numbers between the glaucoma groups (Figure 3.7). However, staining for cleaved caspase 3, a marker for apoptosis, was positive in the GFP-injected glaucoma animals but not present in the XIAP glaucoma group, suggesting some RGCs may be undergoing apoptosis in the GFP group which is inhibited in the XIAP group (Figure 3.8). Furthermore, H&E stains showed visible thinning of the retinal nerve fibre layer (RNFL), which is composed of the axons of the RGCs, in the GFP glaucoma animals, while XIAP glaucoma animals presented with a dense, undamaged layer (Figure 3.9). These results show that although there isn't significant ganglion cell death, there are still signs of potential apoptosis and retinal damage in the GFP glaucoma group, suggesting that the disease pathology is present and progressing.

3.4 XIAP preserves optic nerve and axon structure

Sampled optic nerves were stained with toluidine blue for light microscopy to look for physical differences in the axon structure and counts. Thinning of the RNFL during histological analysis and functional deficits observed in the PERG suggested there should be a similar level of damage in the axons of the GFP glaucoma group. Full cross-sections were examined for differences in morphology, and cross-sectional areas of the optic nerves were measured (Figure 3.10). Analysis of the nerve areas did not yield any significant differences. However, GFP glaucoma animals showed a high degree of glial cell infiltration,

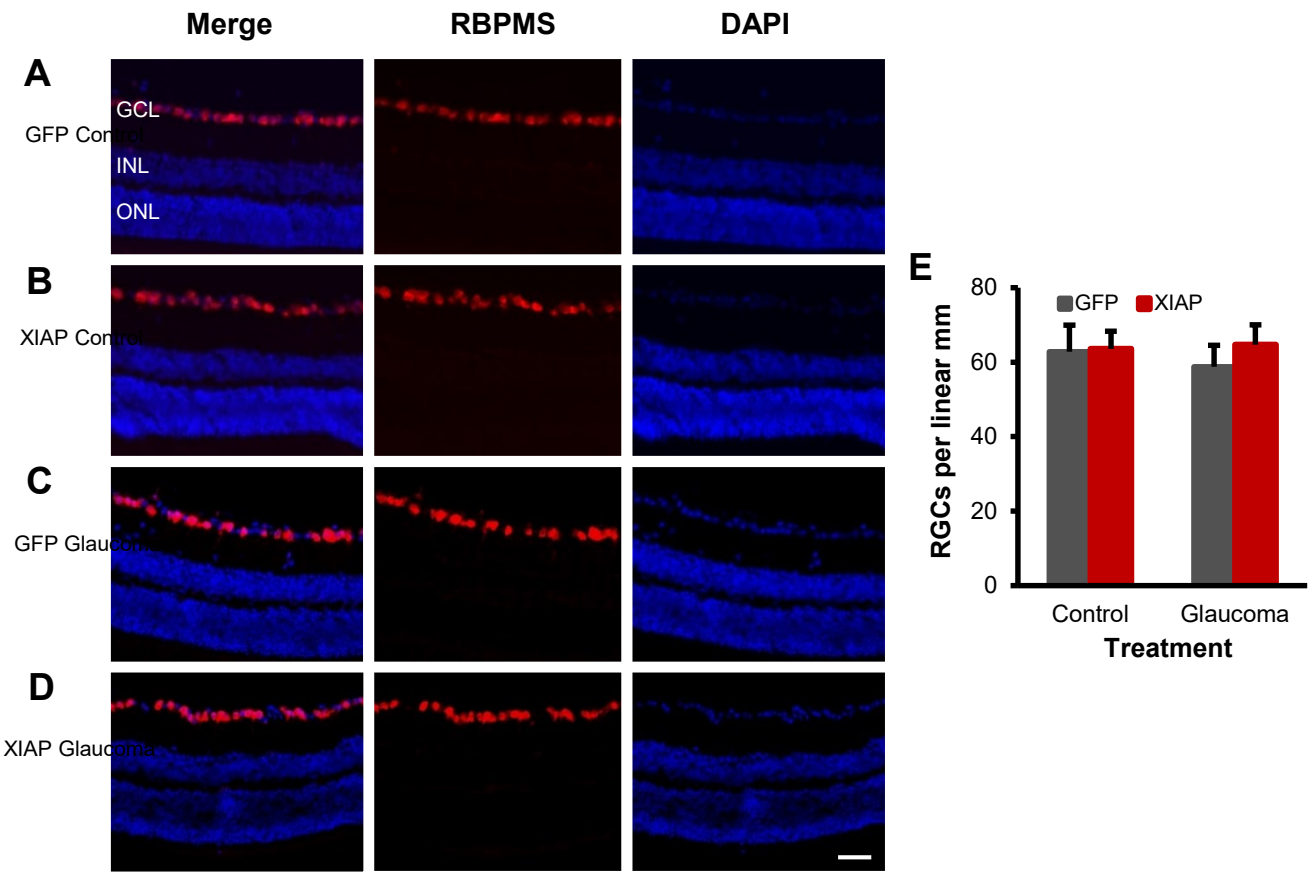

Figure 3.7. RGC somata appear unaffected by IOP elevation. RBPMS staining was done to look at retinal ganglion cell bodies. Retinal sections stained with RBPMS and DAPI in **a)** GFP control, **b)** XIAP control, **c)** GFP glaucoma, and **d)** XIAP glaucoma animals are shown as merged images with individual stains shown beside. **(e)** Mean RGC counts for all four groups show no significant differences. GFP control: n=6; XIAP control: n=6; GFP glaucoma: n=7; XIAP glaucoma: n=8. Error bars = standard deviation. Scale bar: 50 μm

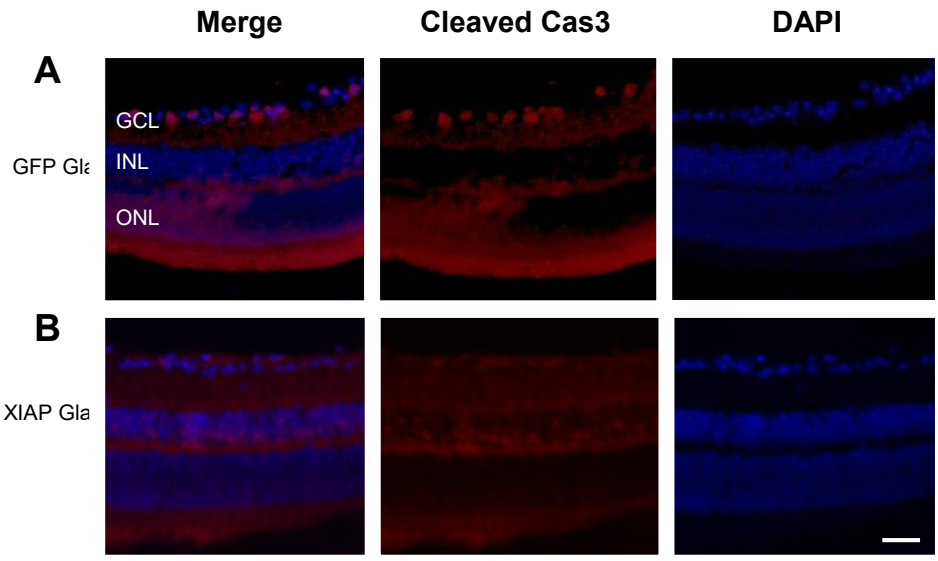

Figure 3.8. GFP glaucoma eyes show signs of apoptosis in GCL. Retinal sections immunostained for cleaved caspase 3 in **a)** GFP glaucoma, and **b)** XIAP glaucoma animals. GFP glaucoma animals stained positive for cleaved caspase 3 in the GCL, a sign of apoptosis, while staining in XIAP glaucoma animals only show background fluorescence. Scale bar: 50 μm.

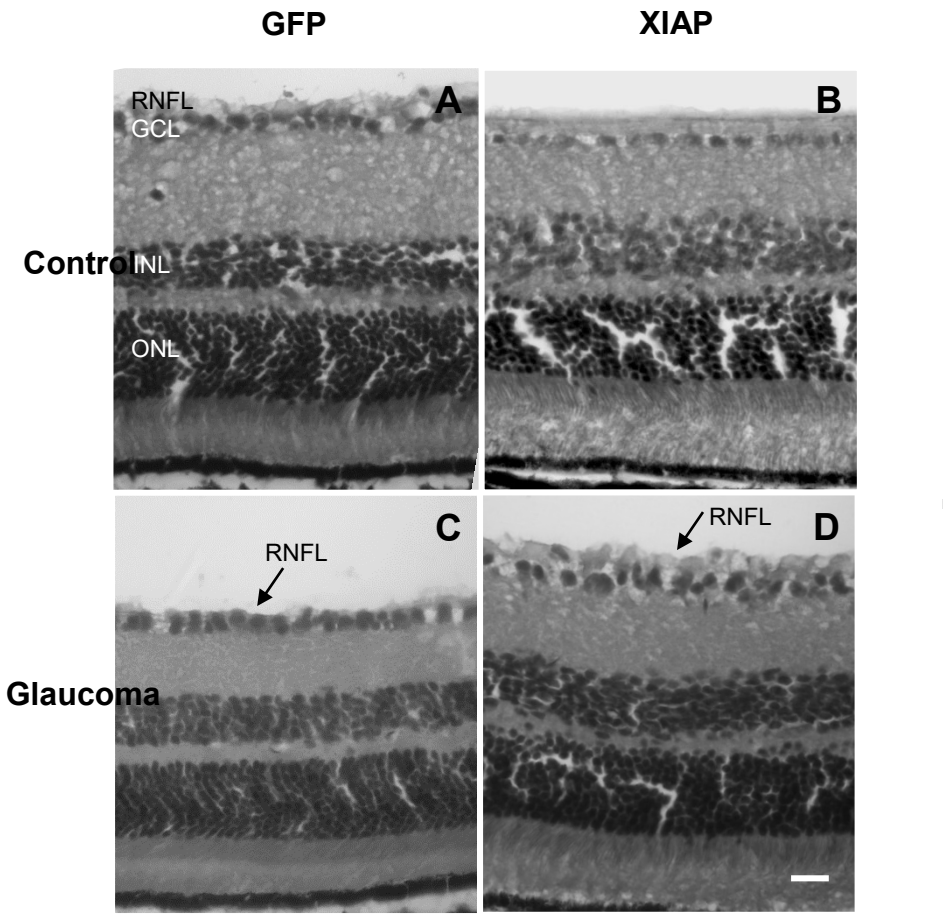

Figure 3.9. GFP glaucoma eyes show significant RNFL thinning, which is prevented in XIAP glaucoma eyes. Retinal sections stained with hematoxylin and eosin in **a)** GFP control, **b)** XIAP control, **c)** GFP glaucoma, and **d)** XIAP glaucoma animals. GFP glaucoma animals present with a highly reduced RNFL (arrow) in comparison to XIAP glaucoma animals, which have RNFLs that are similar to controls. Scale bar: 20 μm.

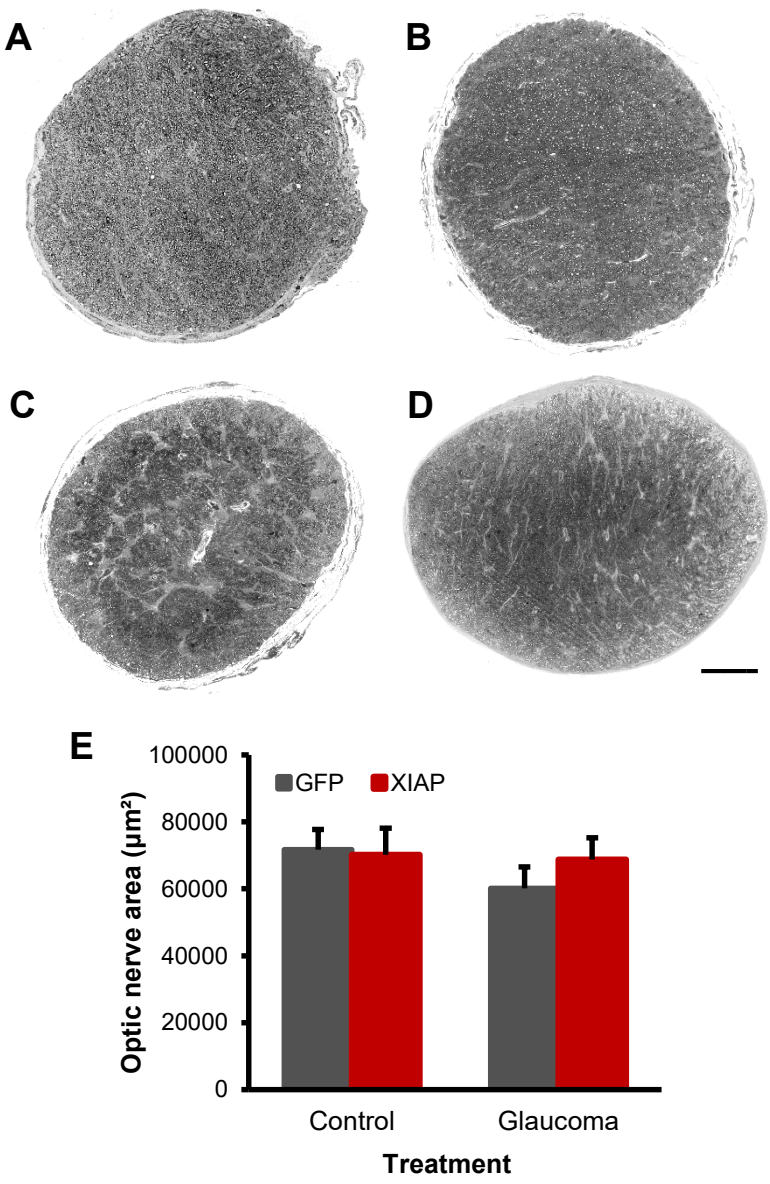

Figure 3.10. GFP glaucoma eyes have greater glial cell coverage and pattern variation with no changes to optic nerve area. Stitched images of entire optic nerve cross-sections stained with toluidine blue from **a)** GFP control, **b)** XIAP control, **c)** GFP glaucoma, and **d)** XIAP glaucoma animals. Optic nerve area measurements show that GFP glaucoma animals do not have significantly different optic nerve areas in comparison to XIAP glaucoma animals. However, GFP glaucoma nerves have increased glial cell infiltration with glial processes appearing to be more disordered, while XIAP glaucoma nerves show decreased gliosis with glial processes taking on a parallel orientation. GFP control: n=3; XIAP control: n=5; GFP glaucoma: n=6; XIAP glaucoma: n=9. Scale bar: 50 µm.

a sign of optic nerve damage, and a difference in glial cell orientation, wherein the cells were highly disorganized with processes not in parallel with one another and following no discernible pattern, which is characteristic of glaucomatous nerves (Cooper et al., 2018). In comparison, XIAP glaucoma animals showed much lower glial cell coverage, with the cells distributed in a parallel orientation.

Glial cell expansion is the result of axon loss (Sofroniew, 2009; Bosco et al., 2016; Cooper et al., 2016). High magnification images of optic nerve cross-sections were taken to look for changes in axon number, density, and morphology. We saw that GFP glaucoma animals reported a reduction of 30% of their axons in comparison to their XIAP counterparts (Figure 3.11). Further examination revealed lower axon density, demyelination, axon swelling, and the presence of darkly stained bodies that are the result of axonal degeneration. However, the disease did not present equally in all tests subjects, and there was some inter-animal variability with the severity of the disease phenotype. Although the animals were all followed for the same length of time following glaucoma induction, animals presented with varying degrees of disease progression. GFP glaucoma animals that showed signs of axon swelling, the presence of apoptotic bodies, and some demyelination, appeared to be in the earlier stages of disease where the pathology is still emerging (Figure 3.11a). Animals that presented with extensive gliosis, a high degree of axon loss, lower axon density, and increased demyelination appeared to be in the later stages, as these signs are suggestive of a higher level of disease severity (Figure 3.11b, c). In contrast, XIAP glaucoma optic nerves were much healthier with much lower phenotypic variability (Figure 3.11d-f). These nerves had more densely packed axons, lower glial cell coverage, fewer apoptotic bodies, no axon swelling or demyelination, and axon counts similar to their BSS controls, all suggesting a significant degree of neuroprotection.

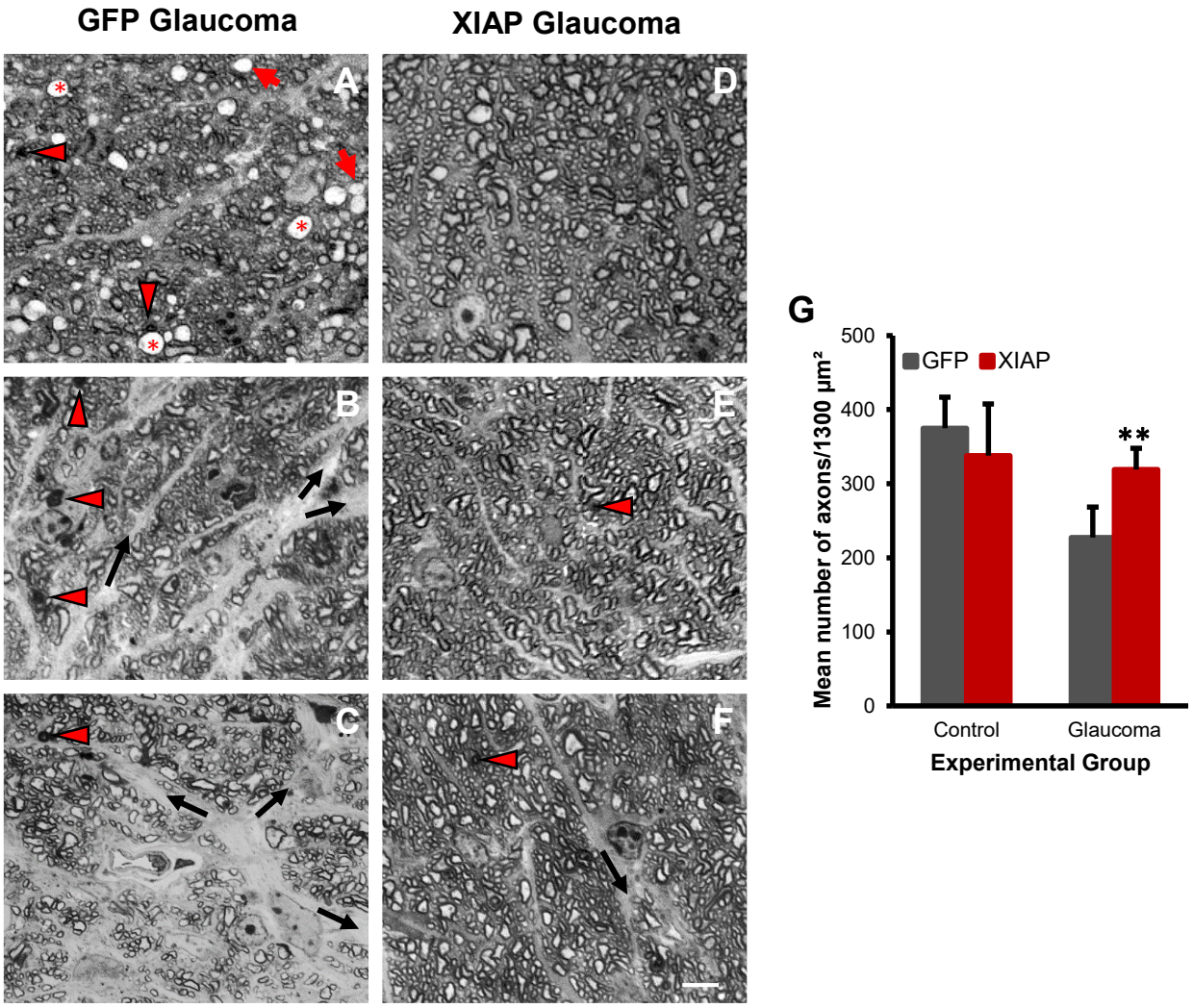

Figure 3.11. Toluidine blue-stained sections reveal increased gliosis and axon loss in GFP glaucoma nerves at varying levels of degeneration. Magnified cross-sections of optic nerves from GFP glaucoma **(a-c)** and XIAP glaucoma **(d-f)** animals. GFP glaucoma nerves show demyelination (red arrows), axonal apoptosis (arrowheads), axonal swelling (asterisks) in the early stages of optic nerve degeneration **(a)**, and as more axons are lost, glial cell processes expand (black arrows) **(b-c)**. In contrast, although XIAP glaucoma nerves show some signs of axonal damage and gliosis, it is reduced in comparison to GFP glaucoma nerves **(d-f)**. **(g)** Mean axon counts reveal that XIAP glaucoma nerves have higher axons numbers than GFP glaucoma nerves. Student's T-test, **p<0.01. Error bars = standard deviation. Scale bar: 10 µm.

To further assess the level of optic nerve damage, three optic nerves from each of the two glaucoma groups were randomly chosen for transmission electron microscopy (TEM). In all cases, GFP glaucoma animals showed greater signs of disease pathology than their XIAP counterparts, including thinner axons, severe axon degeneration, reduced myelination, lower axon density, and increased gliosis (Figure 3.12). The three animals presented with varying degrees of degeneration, and one animal in particular showed severe signs of neurodegeneration (Figure 3.12c). In contrast, XIAP optic nerves had larger, thickly myelinated axons that were more densely packed together with minimal axon loss and glial expansion. These data suggest that XIAP is not only capable of preventing RGCs from dysfunction, but is also able to protect their axons from degeneration.

Overall, GFP glaucoma animals had significantly elevated IOPs, resulting in RGC dysfunction, RNFL thinning, and degeneration and damage of the optic nerve, expanding glial cell infiltration. These changes were variable, with animals exhibiting intermediate to severe levels of damage. However, even with the elevation of IOP, XIAP overexpression preserved RGC activity, prevented RNFL thinning, and protected against axon loss and degeneration, and therefore, glial cell expansion.

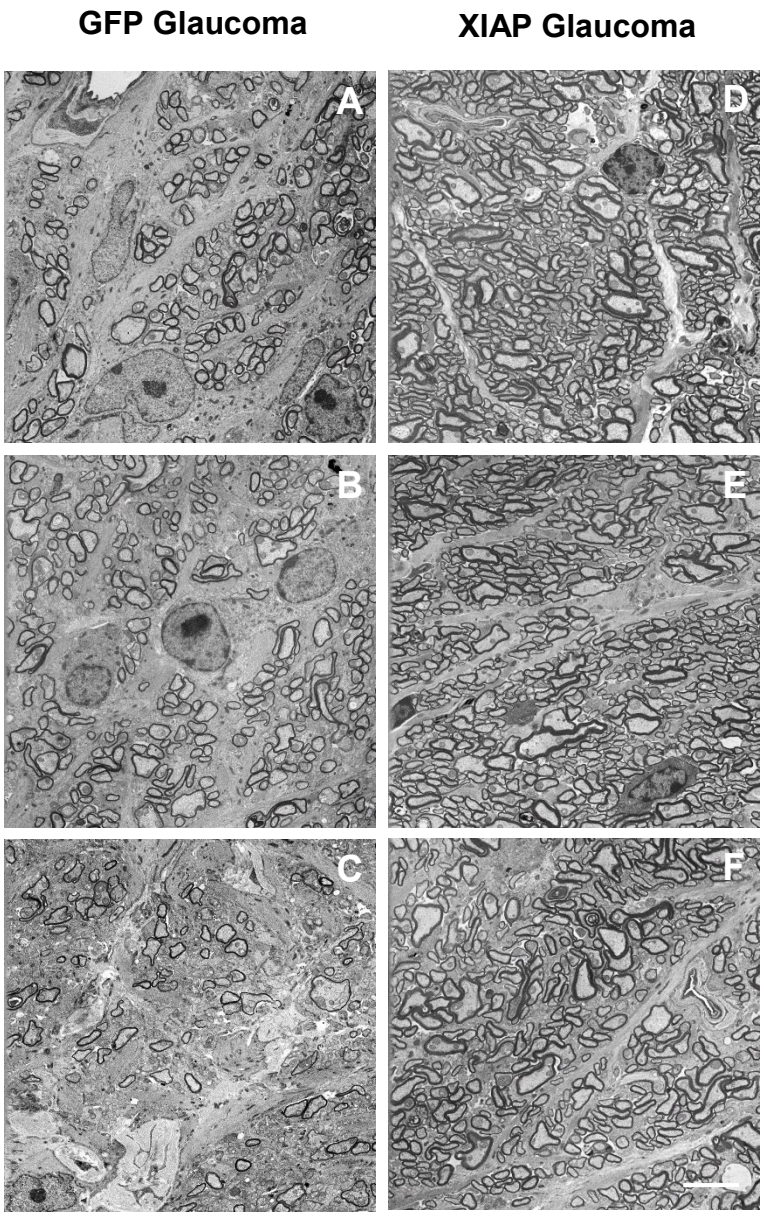

Figure 3.12. Electron microscopy shows that XIAP glaucoma nerves have healthier optic nerve morphology. TEM images of optic nerve cross-sections from GFP glaucoma **(a-c)** and XIAP glaucoma **(d-f)** animals. GFP glaucoma nerves show smaller axons, reduced myelination, severe axon loss, lower axon density, and increased glial expansion **(a-c)**. In contrast, XIAP glaucoma nerves show larger axons, thicker myelination, more axons at a higher density, and fewer glial processes **(d-f)**. Scale bar: 5 μm.

4.0 DISCUSSION

This thesis examined the ability of XIAP to protect RGCs and their axons from damage in a model of ocular hypertension. Our study showed that XIAP was successfully able to preserve RGC and optic nerve function and structure, maintaining RGC activity and inhibiting axonal death and damage. In comparison to their GFP-treated controls, XIAP-injected glaucoma animals had more robust ganglion cell responses, thicker RNFLs, and minimal caspase 3 activation. Furthermore, XIAP-treated optic nerves were composed of densely-packed, well-myelinated axons, and showed minimal degeneration and glial cell infiltration, suggesting that the therapy is functionally and structurally protective.

Many studies have established that the ultimate endpoint of glaucoma is ganglion cell death, primarily via apoptosis, so we chose XIAP as the therapy we wanted to test because of its potent caspase inhibition activity (Shiozaki et al., 2003; Scott et al., 2005; Chai et al., 2001., Quinn et al., 1997). XIAP's neuroprotective abilities have previously been tested in various *in vivo* and *in vitro* models of retinal cell death, all showing some level of neuroprotection with XIAP overexpression (Renwick et al., 2006; Leonard et al., 2007; Zadro-Lamoureux et al., 2009). One study in particular specifically looked at XIAP overexpression in a rat model of IOP elevation with injections of hypertonic saline to sclerose the episcleral veins to prevent aqueous outflow and showed signs of neuroprotection (McKinnon et al., 2002). However, while the XIAP-injected animals showed improvements in optic nerve structure, there were no tests performed to assess neuronal or axonal function. The authors also observed highly variable IOP elevations between animals and large fluctuations in pressure. To test XIAP in our lab, we chose a model developed by Ito et al. (2016) for its acute IOP elevation, reduced monitoring length, easier induction technique, and how little the IOP increase varied from mouse to mouse. Similar to the authors, we

observed little variability in IOP elevation, and witnessed functional changes in RGCs starting at as soon as three weeks-post glaucoma induction.

McKinnon et al. (2012) also reported lower IOPs in the XIAP-injected glaucoma rats. In our model, we observed that XIAP glaucoma animals showed no differences in IOP elevation rates when compared to the GFP glaucoma animals, with both groups showing significantly elevated IOP compared to their BSS controls. In their study, McKinnon et al. (2002) hypothesized that XIAP was preventing the apoptosis of important cells in the trabecular meshwork, thus interfering with IOP elevation, which would require that some of the intravitreally-injected virus travelled or was transported into the anterior chamber to infect these cells. This hypothesis is a possibility in the hypertonic saline model, because the injections sclerose the veins, leading to vascular dysregulation and increased cell death in the trabecular meshwork (TM) via oxidative damage (Alvarado et al., 1984). However, in our model, the beads are a physical block against the TM, unable to damage the TM cells or affect the ocular vasculature enough to promote oxidative stress. XIAP cannot function to prevent TM damage and slow IOP elevation in such a scenario.

As previously mentioned, we observed a significant rise in IOP one week following bead injections in our glaucoma animals that was sustained, which was similar to the results of the developers of the model. There were, however, differences in the magnitude of IOP elevation. Ito et al. (2016) reported a mean increase in IOP from 10 mmHg to 20 mmHg while in our study, the animals reported much lower readings. These differences were caused by our use of anesthesia to record IOP measurements. The Tono-Pen records measurements by placing the pen directly on the cornea to take readings. Awake mice required restraining, which stressed the mice and elevated their IOPs, providing inaccurate and variable recordings. Mice were also uncomfortable with the direct corneal contact and

would jerk, sometimes resulting in damage to the eye. However, anesthetic use has its own caveats, as it reduces their heart rate and stress, thereby lowering the IOP. A study looking at the effect of various anesthetics on the IOPs of normal and glaucomatous eyes reported a 48% decrease in IOP in normal C57BL/6J mice 30 minutes after they were anesthetized with ketamine, which was more pronounced in mice with bead-induced IOP elevation where the decrease was nearly 64% (Ding et al., 2011). The study showed that IOP recordings taken after anesthetizing the animals underestimate the actual pressure, and that the decrease is inversely proportional to the IOP level. These results would explain the modest IOP increases we observed in the anesthetized glaucoma animals in our study, suggesting that their actual IOPs were much higher than the anesthetized IOPs that were recorded.

Although we recorded IOPs that were lower than those reported in the original study, we were still able to see statistically significant and sustained elevation in the glaucoma animals when compared to their BSS controls. We also noticed significant changes in the histology and activity of the optic nerves and retinas of XIAP-injected animals compared to those injected with the GFP vector. Functional testing showed that XIAP overexpression appeared to prevent RGC dysfunction. Monitoring RGC activity was an important aspect of this study, as we already had evidence suggesting XIAP was capable of structural protection in a glaucoma model (McKinnon et al., 2002). Although preservation of the ganglion cell bodies is an important aspect of protection, it was also necessary to test whether the neurons were only saved from cell death or if they could respond normally as well. Analysis of our data at six weeks after glaucoma surgeries revealed that XIAP glaucoma RGCs recorded functional responses similar to the BSS-injected controls, while GFP glaucoma RGC activity was significantly impaired (Figure 3.5). It is evident that XIAP is not only protecting the cells from apoptosis or other forms of cell death, but is also preventing the cells from dysfunction. While XIAP was primarily chosen for its role in inhibiting caspase-

dependent cell death, it also interacts with key enzymes and complexes in several caspase-independent damage pathways, one of which is oxidative stress. In glaucomatous optic neuropathy, vascular dysregulation in the retina and optic nerve (Gherghel et al., 2000) and unstable ocular blood flow results in repeated mild reperfusion injury, creating chronic oxidative stress in the optic nerve head (ONH) (Flammer, 2001). The mechanical stress from the elevated IOP also activates astrocytes, producing nitric oxide radicals (Neufeld et al, 1997). These radicals coupled with the superoxide that the ONH mitochondria produce as a result of reperfusion injury form the highly damaging peroxynitrite (Flammer and Mozaffarieh, 2007). All three ROS can diffuse within the axons and be transported retrogradely to the retina, resulting in oxidative damage to both the axons and somata of the RGCs. XIAP indirectly suppresses ROS accumulation by activating NF-κB in a caspase-independent manner, leading to increased SOD antioxidant production (Evans et al., 2016). By contributing to the elimination of these radicals, XIAP can minimize RGC somal and axonal damage, protecting against loss of function.

While tests for the RGC somata and axons showed differences between the two glaucoma groups, results for other retinal cells did not show any differences, suggesting that the model did not penetrate beyond the GCL and affect deeper retinal layers. Previous studies looking at neurons affected by glaucoma have shown that RGCs are the cells primarily lost in the disease, especially at the early stages, so we do not expect functional or structural changes beyond the GCL. However, seeing as the model should result in axonal degeneration, which affects signalling from the optic nerve to the visual cortex, we did expect to see differences in the VEP test, particularly after the results from the histology showed significant axon loss in the GFP glaucoma animals. One hypothesis for the preservation of the VEPs in our GFP glaucoma animals is that although the axonal degeneration was significant, the remaining axons may have compensated for the loss, remaining functional enough to propagate the signalling through the nerve to

the cortex and elicit a response. We also noticed significant variability and non-uniformity in our traces, more so than any other functional test we used. Trace variability may have been caused by errors in manual setup, i.e., imperfect subdermal placement of the electrode on the visual cortex, or dislodging of the electrode during the test. We also used a flash VEP instead of a pattern VEP to test optic nerve integrity. Current clinical practice elects to use the pattern VEP over the flash VEP for glaucoma patient testing for many reasons, one of which is that pattern VEPs are more sensitive in detecting subtle optic neuropathies like glaucoma than flash VEPs (Jha et al., 2017). We also observed no differences in latency when testing with the flash VEP. Besides reduced pattern VEP amplitudes, glaucoma patients also exhibit longer pattern VEP latencies, which are used as an early detector for the disease (Atkin et al., 1983; Parisi, 1997; Parisi et al., 2006). Very few studies show flash VEP usage in patients; however, one study noted significant amplitude reductions in the P1 component of the flash VEP tests of glaucoma patients compared to normal patients (Watts et al., 1989), which we did not see in our animals. It is possible that while the flash VEP might have reported deficits in signalling integrity in patients, it may not be directly translatable for use in other species, as we have observed in our lab with another test, the uniform field on/off flash ERG (Lagali et al., 2018; manuscript in preparation). Georgiou et al. (2014) previously tested the simultaneous flash ERG and VEP test used in our study in an ocular hypertensive rat model and, although they reported significant RNFL and RGC loss, they did not see differences in VEP amplitude. These results suggest that the flash VEP might not be the most ideal method for testing in rodent models of glaucoma. Moving forward, testing the pattern VEP in this model might result in more reliable traces and give us two parameters, amplitude and latency, to measure functional decline.

Alongside functional preservation, XIAP overexpression was also structurally protective in the glaucoma model; retinal histology revealed that XIAP glaucoma animals retained RNFL thickness and

showed little-to-no caspase 3 activation. However, we were unable to replicate the significant RGC loss reported by the developers of the model, starting three weeks following glaucoma induction. Although ganglion cell counts were not different between the two glaucoma groups, we did observe other signs of damage in the RNFL and the RGC bodies in the GFP-injected animals. A six-week timespan was enough to see thinning of the RNFL and caspase activation in the GCL of the GFP glaucoma animals, suggesting that the model's IOP elevation was significant enough to start the damage. Furthermore, analysis of the optic nerves revealed significant signs of axon loss in the GFP glaucoma animals compared to the XIAP group. In glaucoma, pressure rise interferes with axoplasmic flow, with abolishment of anterograde transport preceding dysfunction in retrograde transport; axon transport failure initiates distally, eventually progressing to proximal sites in the optic nerve head and retina (Crish et al., 2010). RGC somata are unable to supplement axons with neurotrophic factors, and transport deficiencies eventually lead to axonal degeneration (Caleo et al., 2000), which precedes RGC apoptosis (Buckingham et al., 2008). Transport failure, axonal degeneration, dendrite remodeling, and RGC shrinkage all precede ganglion cell death, suggesting there is a cascade of events (Jakobs et al., 2005). Histological evidence suggests that the disease was still progressing in our animals and would have ultimately led to RGC loss. It is also important to note that endogenous XIAP is upregulated in glaucomatous retinas but downregulated in glaucomatous optic nerves, which may explain the increased damage susceptibility of the optic nerve axons compared to the RGC somata; the cell bodies have a layer of protection against apoptotic damage that the axons lack (Levkovitch-Verbin et al., 2013a). Although we did not test for differences in XIAP expression or protein level in this study, future studies may want to see if XIAP-injected animals show a similar uneven distribution of XIAP in RGC somata versus their axons.

It is important to consider that although XIAP was shown to be able to protect the structural integrity of the optic nerve and the retina in this study, moving forward, changes must be made to the experimental design to make it more clinically relevant. This study was conducted as a proof-of-principle to test XIAP's ability to preserve retinal and neural activity and structure in a model of ocular hypertension. As such, we injected our animals with the gene therapy three weeks prior to glaucoma induction to allow XIAP to be optimally expressed before the onset of the disease, particularly because the monitoring period following the injection of microbeads was only six weeks long. Future studies may want to test XIAP's neuroprotective abilities in a chronic model, such as the genetic DBA/2J model, where the therapy can be applied following disease onset to understand further the mechanisms of XIAP protection in glaucoma. Testing the therapy in this model would also take into consideration another significant factor in glaucoma: age. It is well-documented that old age naturally results in RGC loss and axon degeneration (Balazsi et al., 1984; Harman et al., 2000). In glaucoma, susceptibility to axonal transport deficits increases with age and appears unrelated to elevated IOP (Crish et al., 2010). Although elevated IOP is generally considered to be the greatest risk factor and the major therapeutic target, approximately 50% of all glaucoma is not caused by it (Shields, 2008). More importantly, under similar IOP levels, aged glaucoma mice reported significantly decreased XIAP and IAP-1 levels, while young glaucoma mice showed a significant upregulation of both genes (Levkovitch-Verbin et al., 2013b), suggesting aging disrupts a built-in repair mechanism and increases susceptibility to damage. Using an aged model with longer monitoring periods would also be useful in testing whether XIAP is capable of preventing degeneration in the retina and optic nerve with sustained exposure to elevated IOP, as we tested the therapy for only six weeks in the glaucoma model. It is clear that we see evidence of neuroprotection with XIAP overexpression in an acute model using young mice, but moving forward, we

may want to test the transgene's ability to preserve RGC axons and somata in aged mice using a chronic model to see if it is beneficial then as well.

Another factor to consider is the overall protective efficacy of XIAP in glaucoma. Functional and structural analysis showed evidence of retina and optic nerve preservation in XIAP-injected glaucoma animals when compared to the GFP glaucoma controls. However, it was clear that XIAP overexpression resulted in an incomplete rescue and led to some variability in protection. Although we did not analyze XIAP expression levels, McKinnon et al. (2002) reported major inter-animal differences in XIAP mRNA levels after AAV-mediated gene delivery, suggesting these differences may have caused the variability in XIAP-mediated protection. As previously stated, future studies may benefit from testing XIAP mRNA at both the retina and the optic nerve, measuring expression levels pre- and post viral delivery. Furthermore, although we were able to prevent various forms of cell death via XIAP overexpression, glaucoma is a multifactorial disease (Agarwal et al., 2009) and viable long-term options to protect vision would have to look towards combination therapies, particularly because XIAP is neuroprotective but not regenerative. Known factors that contribute to disease pathology besides elevated IOP include autophagy (Deng et al., 2013), inflammation (Williams et al., 2017), oxidative stress (Izzotti et al., 2006), excitotoxicity (Osborne, 2008), and loss of trophic support (Johnson et al., 2009). Both oxidative stress and glutamate toxicity are relevant in all glaucomas, but they are primary mechanisms of damage in glaucomas that develop independently of IOP elevation (Gherghel et al., 2000; Harada et al., 2010), and are therefore important therapeutic targets to consider. Studies in our lab are currently looking into the synergistic effects of the antioxidant, 2-[mesityl(methyl)amino]-N-[4-(pyridin-2-yl)-1H-imidazol-2-yl] acetamide trihydrochloride (WN1316), coupled with XIAP in a model of Leber's hereditary optic neuropathy (LHON). Treatment with WN1316 effectively reduced cell death in a neuroblastoma cell line

in vitro alone and synergistically with XIAP, suggesting combination therapy in *in vivo* models may be successful. Besides inducing oxidative stress, elevated IOP also leads to neurotrophic deficits, another major degenerative element. Loss of neurotrophic factors is the result of impaired axonal transport, which precipitates the remaining pathways leading to glaucomatous damage. Providing trophic support through injections of purified neurotrophins has been shown to promote RGC survival (Ma et al., 1998; Galindo-Romero et al., 2013). Neurotrophin delivery has been a key area of study in glaucoma treatments because they have also been implicated in stimulating axon regeneration (Müller et al., 2009; Lingor et al., 2008), by working synergistically to terminate inhibition of growth pathways (Logan et al., 2006). Ultimately, the ideal treatment would combine the two strategies of neuroregeneration and neuroprotection alongside IOP lowering to provide maximal therapeutic benefit to glaucoma patients. Supplying trophic factors to extend and support axons in combination with an agent capable of inhibiting degeneration pathways would be an excellent way to combat disease progression and preserve vision.

This study was a promising look into the therapeutic potential of XIAP in patients with glaucoma. XIAP overexpression yielded structural and functional protection of both the retina and the optic nerve in an acute glaucoma model, providing proof-of-principle. However, further studies are required in multiple glaucoma models to assess the full extent of XIAP's neuroprotective abilities before it can be considered as an effective therapy. As of now, the results of this study are an important step forward in evaluating XIAP as a treatment for glaucoma.

REFERENCES

Abu-Hassan, D. W., Acott, T. S. & Kelley, M. J. The trabecular meshwork: a basic review of form and function. *J Ocul Biol* **2**, (2014).

Acott, T. S. *et al.* Intraocular pressure homeostasis: maintaining balance in a high-pressure environment. *J Ocul Pharmacol Ther* **30**, 94-101 (2014).

Acott, T. S. & Kelley, M. J. Extracellular matrix in the trabecular meshwork. *Exp Eye Res* **86**, 543-561 (2008).

Agarwal, R., Gupta, S. K., Agarwal, P., Saxena, R. & Agrawal, S. S. Current concepts in the pathophysiology of glaucoma. *Indian J Ophthalmol* **57**, 257-266 (2009).

Ajibade, A. A., Wang, H. Y. & Wang, R.-F. Cell type-specific function of TAK1 in innate immune signaling. *Trends Immunol* **34**, 307-316 (2013).

Alvarado, J., Murphy, C. & Juster, R. Trabecular meshwork cellularity in primary open-angle glaucoma and nonglaucomatous normals. *Ophthalmology* **91**, 564-579 (1984).

Amerasinghe, N. *et al.* The heritability and sibling risk of angle closure in Asians. *Ophthalmology* **118**, 480-485 (2011).

Anderson, D. R. Ultrastructure of human and monkey lamina cribrosa and optic nerve head. *Arch Ophthalmol* **82**, 800-814 (1969).

Anderson, M. G. *et al.* Mutations in genes encoding melanosomal proteins cause pigmentary glaucoma in DBA/2J mice. *Nat Genet* **30**, 81-85 (2002).

Ashkenazi, A. & Dixit, V. M. Death receptors: signaling and modulation. *Science* **281**, 1305-1308 (1998).

Atkin, A. *et al.* Flicker threshold and pattern VEP latency in ocular hypertension and glaucoma. *Invest Ophthalmol Vis Sci* **24**, 1524-1528 (1983).

Balazsi, A. G., Rootman, J., Drance, S. M., Schulzer, M. & Douglas, G. R. The effect of age on the nerve fiber population of the human optic nerve. *Am J Ophthalmol* **97**, 760-766 (1984).

Bartesaghi, S., Marinovich, M., Corsini, E., Galli, C. L. & Viviani, B. Erythropoietin: a novel neuroprotective cytokine. *Neurotoxicology* **26**, 923-928 (2005).

Baseler, H. A. & Sutter, E. E. M and P components of the VEP and their visual field distribution. *Vision Res* **37**, 675-690 (1997).

Benoist d'Azy, C., Pereira, B., Chiambaretta, F. & Dutheil, F. Oxidative and anti-oxidative stress markers in chronic glaucoma: a systematic review and meta-analysis. *PLoS ONE* **11**, e0166915 (2016).

Bosco, A. *et al.* Glial coverage in the optic nerve expands in proportion to optic axon loss in chronic mouse glaucoma. *Exp Eye Res* **150**, 34-43 (2016).

Brubaker, R. F. Delayed functional loss in glaucoma. LII Edward Jackson Memorial Lecture. *Am J Ophthalmol* **121**, 473-483 (1996).

Buckingham, B. P. *et al.* Progressive ganglion cell degeneration precedes neuronal loss in a mouse model of glaucoma. *J Neurosci* **28**, 2735-2744 (2008).

Caleo, M., Menna, E., Chierzi, S., Cenni, M. C. & Maffei, L. Brain-derived neurotrophic factor is an anterograde survival factor in the rat visual system. *Curr Biol* **10**, 1155-1161 (2000).

Chai, J. *et al.* Structural basis of caspase-7 inhibition by XIAP. *Cell* **104**, 769-780 (2001).

Chai, J. *et al.* Structural and biochemical basis of apoptotic activation by Smac/DIABLO. *Nature* **406**, 855-862 (2000).

Chen, H. & Weber, A. J. BDNF enhances retinal ganglion cell survival in cats with optic nerve damage. *Invest Ophthalmol Vis Sci* **42**, 966-974 (2001).

Chidlow, G., Ebneter, A., Wood, J. P. M. & Casson, R. J. The optic nerve head is the site of axonal transport disruption, axonal cytoskeleton damage and putative axonal regeneration failure in a rat model of glaucoma. *Acta Neuropathol* **121**, 737-751 (2011).

Cho, H. & Kee, C. Population-based glaucoma prevalence studies in Asians. *Surv Ophthalmol* **59**, 434-447 (2014).

Clark, M. E. & Kraft, T. W. Measuring rodent electroretinograms to assess retinal function. *Methods Mol Biol* **884**, 265-276 (2012).

Cohen, G. M. Caspases: the executioners of apoptosis. *Biochem J* **326** (Pt 1), 1-16 (1997).

Collaborative Normal-Tension Glaucoma Study Group. The effectiveness of intraocular pressure reduction in the treatment of normal-tension glaucoma. *Am J Ophthalmol* **126**, 498-505 (1998).

Cooper, M. L., Collyer, J. W. & Calkins, D. J. Astrocyte remodeling without gliosis precedes optic nerve Axonopathy. *Acta Neuropathol Commun* **6**, (2018).

Cooper, M. L., Crish, S. D., Inman, D. M., Horner, P. J. & Calkins, D. J. Early astrocyte redistribution in the optic nerve precedes axonopathy in the DBA/2J mouse model of glaucoma. *Exp Eye Res* **150**, 22-33 (2016).

Crish, S. D., Sappington, R. M., Inman, D. M., Horner, P. J. & Calkins, D. J. Distal axonopathy with structural persistence in glaucomatous neurodegeneration. *Proc Natl Acad Sci U S A* **107**, 5196-5201 (2010).

Damgaard, R. B. *et al.* Disease-causing mutations in the XIAP BIR2 domain impair NOD2-dependent immune signalling. *EMBO Mol Med* **5**, 1278-1295 (2013).

Danesh-Meyer, H. V. & Levin, L. A. Neuroprotection: extrapolating from neurologic diseases to the eye. *Am J Ophthalmol* **148**, 186-191.e2 (2009).

De La Paz, M. A. & Epstein, D. L. Effect of age on superoxide dismutase activity of human trabecular meshwork. *Invest Ophthalmol Vis Sci* **37**, 1849-1853 (1996).

Deng, S. *et al.* Autophagy in retinal ganglion cells in a rhesus monkey chronic hypertensive glaucoma model. *PLoS ONE* **8**, e77100 (2013).

Di Polo, A., Aigner, L. J., Dunn, R. J., Bray, G. M. & Aguayo, A. J. Prolonged delivery of brain-derived neurotrophic factor by adenovirus-infected Müller cells temporarily rescues injured retinal ganglion cells. *Proc Natl Acad Sci U S A* **95**, 3978-3983 (1998).

Ding, C., Wang, P. & Tian, N. Effect of general anesthetics on IOP in elevated IOP mouse model. *Exp Eye Res* **92**, 512-520 (2011).

Donati, S. *et al.* Vitreous substitutes: the present and the future. *Biomed Res Int* **2014**, 351804 (2014).

Doozandeh, A. & Yazdani, S. Neuroprotection in glaucoma. *J Ophthalmic Vis Res* **11**, 209-220 (2016).

Erskine, L. & Herrera, E. Connecting the retina to the brain. *ASN Neuro* **6**: 175909141456210 (2014).

Evans, M. K. *et al.* X-linked inhibitor of apoptosis protein mediates tumor cell resistance to antibody-dependent cellular cytotoxicity. *Cell Death Dis* **7**, e2073 (2016).

Fahy, E. T., Chrysostomou, V. & Crowston, J. G. Mini-review: impaired axonal transport and glaucoma. *Curr Eye Res* **41**, 273-283 (2016).

Fang, J. H., Wang, X. H., Xu, Z. R. & Jiang, F. G. Neuroprotective effects of bis(7)-tacrine against glutamate-induced retinal ganglion cells damage. *BMC Neurosci* **11**, 31 (2010).

Ferreira, S. M. *et al.* Time course changes of oxidative stress markers in a rat experimental glaucoma model. *Invest Ophthalmol Vis Sci* **51**, 4635-4640 (2010).

Flammer, J. [Glaucomatous optic neuropathy: a reperfusion injury]. *Klin Monbl Augenheilkd* **218**, 290291 (2001).

Flammer, J. & Mozaffarieh, M. What is the present pathogenetic concept of glaucomatous optic neuropathy? *Surv Ophthalmol* **52** Suppl 2, S162-173 (2007).

Fortune, B. *et al.* Selective ganglion cell functional loss in rats with experimental glaucoma. *Invest Ophthalmol Vis Sci* **45**, 1854-1862 (2004).

Gaillard, F. Optic nerve I Radiology Reference Article I Radiopaedia.org. *Radiopaedia* Available at: https://radiopaedia.org/articles/optic-nerve. (Accessed: 31st October 2018)

Galbán, S. & Duckett, C. S. XIAP as a ubiquitin ligase in cellular signaling. *Cell Death Differ* **17**, 54-60 (2010).

Galindo-Romero, C. *et al.* Effect of brain-derived neurotrophic factor on mouse axotomized retinal ganglion cells and phagocytic microglia. *Invest Ophthalmol Vis Sci* **54**, 974-985 (2013).

Garcia-Valenzuela, E., Shareef, S., Walsh, J. & Sharma, S. C. Programmed cell death of retinal ganglion cells during experimental glaucoma. *Exp Eye Res* **61**, 33-44 (1995).

Georgiou, A. L., Guo, L., Francesca Cordeiro, M. & Salt, T. E. Electroretinogram and visual-evoked potential assessment of retinal and central visual function in a rat ocular hypertension model of glaucoma. *Curr Eye Res* **39**, 472-486 (2014).

Gherghel, D., Orgill, S., Gugleta, K., Gekkieva, M. & Flammer, J. Relationship between ocular perfusion pressure and retrobulbar blood flow in patients with glaucoma with progressive damage. *Am J Ophthalmol* **130**, 597-605 (2000).

Goel, M., Picciani, R. G., Lee, R. K. & Bhattacharya, S. K. Aqueous humor dynamics: a review. *Open Ophthalmol J* **4**, 52-59 (2010).

Guo, L. *et al.* Retinal ganglion cell apoptosis in glaucoma is related to intraocular pressure and TOP-induced effects on extracellular matrix. *Invest Ophthalmol Vis Sci* **46**, 175-182 (2005).

Harada, C. *et al.* ASK1 deficiency attenuates neural cell death in GLAST-deficient mice, a model of normal tension glaucoma. *Cell Death Differ* **17**, 1751-1759 (2010).

Harman, A., Abrahams, B., Moore, S. & Hoskins, R. Neuronal density in the human retinal ganglion cell layer from 16-77 years. *Anat Rec* **260**, 124-131 (2000).

Hauswirth, W. W., Lewin, A. S., Zolotukhin, S. & Muzyczka, N. Production and purification of recombinant adeno-associated virus. *Meth Enzymol* **316**, 743-761 (2000).

Hennis, A. *et al.* Awareness of incident open-angle glaucoma in a population study: the Barbados Eye Studies. *Ophthalmology* **114**, 1816-1821 (2007).

Hernandez, M. R. The optic nerve head in glaucoma: role of astrocytes in tissue remodeling. *Prog Ret Eye Res* **19**, 297-321 (2000).

Hill, M. M., Adrain, C., Duriez, P. J., Creagh, E. M. & Martin, S. J. Analysis of the composition, assembly kinetics and activity of native Apaf-1 apoptosomes. *EMBO J* **23**, 2134-2145 (2004).

Holcik, M. & Korneluk, R. G. XIAP, the guardian angel. *Nat Rev Mol Cell Bio* **2**, 550-556 (2001).

Holder, G. E. Pattern electroretinography (PERG) and an integrated approach to visual pathway diagnosis. *Prog Ret Eye Res* **20**, 531-561 (2001).

Huang, *Y. et al.* Structural basis of caspase inhibition by XIAP: differential roles of the linker versus the BIR domain. *Cell* **104**, 781-790 (2001).

Ito, Y. A., Belforte, N., Cueva Vargas, J. L. & Di Polo, A. A magnetic microbead occlusion model to induce ocular hypertension-dependent glaucoma in mice. *J Vis Exp* **109**, e53731 (2016).

Izzotti, A., Bagnis, A. & Sacca, S. C. The role of oxidative stress in glaucoma. *Mutat Res-Rev Mutat* **612**, 105-114 (2006).

Izzotti, A., Sacca, S. C., Cartiglia, C. & De Flora, S. Oxidative deoxyribonucleic acid damage in the eyes of glaucoma patients. *Am J Med*, 638-646 (2003).

Jakobs, T. C., Libby, R. T., Ben, Y., John, S. W. M. & Masland, R. H. Retinal ganglion cell degeneration is topological but not cell type specific in DBA/1142J mice. *J Cell Biol* **171**, 313-325 (2005).

Jha, M. K., Thakur, D., Limbu, N., Badhu, B. P. & Paudel, B. H. Visual evoked potentials in primary open angle glaucoma. *J Neurodegener Dis* **2017**, 9540609 (2017).

Johnson, E. C., Guo, Y., Cepurna, W. 0. & Morrison, J. C. Neurotrophin roles in retinal ganglion cell survival: lessons from rat glaucoma models. *Exp Eye Res* **88**, 808-815 (2009).

Johnson, J. E., Barde, Y. A., Schwab, M. & Thoenen, H. Brain-derived neurotrophic factor supports the survival of cultured rat retinal ganglion cells. *J Neurosci* **6**, 3031-3038 (1986).

Johnston, M. C., Noden, D. M., Hazelton, R. D., Coulombre, J. L. & Coulombre, A. J. Origins of avian ocular and periocular tissues. *Exp Eye Res* **29**, 27-43 (1979).

Ju, W.-K. *et al.* Intraocular pressure elevation induces mitochondrial fission and triggers OPAL release in glaucomatous optic nerve. *Invest Ophthalmol Vis Sci* **49**, 4903-4911 (2008).

Kahn, M. G., Giblin, F. J. & Epstein, D. L. Glutathione in calf trabecular meshwork and its relation to aqueous humor outflow facility. *Invest Ophthalmol Vis Sci* **24**, 1283-1287 (1983).

Kerr, J. F., Wyllie, A. H. & Currie, A. R. Apoptosis: a basic biological phenomenon with wide-ranging implications in tissue kinetics. *Br J Cancer* **26**, 239-257 (1972).

Kerrigan, L. A., Zack, D. J., Quigley, H. A., Smith, S. D. & Pease, M. E. TUNEL-positive ganglion cells in human primary open-angle glaucoma. *Arch Ophthalmol* **115**, 1031-1035 (1997).

Kischkel, F. C. *et al.* Cytotoxicity-dependent APO-1 (Fas/CD95)-associated proteins form a death-inducing signaling complex (DISC) with the receptor. *EMBO J* **14**, 5579-5588 (1995).

Klein, B. E. K. *et al.* Prevalence of glaucoma: The Beaver Dam Eye Study. *Ophthalmology* **99**, 1499-1504 (1992).

Ko, M.-L., Peng, P.-H., Ma, M.-C., Ritch, R. & Chen, C.-F. Dynamic changes in reactive oxygen species and antioxidant levels in retinas in experimental glaucoma. *Free Radical Bio Med* **39**, 365-373 (2005).

Kwon, Y. H., Fingert, J. H., Kuehn, M. H. & Alward, W. L. M. Primary open-angle glaucoma. *N Engl J Med* **360**, 1113-1124 (2009).

Lascaratos, G., Garway-Heath, D. F., Willoughby, C. E., Chau, K.-Y. & Schapira, A. H. V. Mitochondrial dysfunction in glaucoma: understanding genetic influences. *Mitochondrion* **12**, 202-212 (2012).

Leonard, K. C. *et al.* XIAP protection of photoreceptors in animal models of retinitis pigmentosa. *PLoS ONE* **2**, e314 (2007).

Levkovitch-Verbin, H., Makarovsky, D. & Vander, S. Comparison between axonal and retinal ganglion cell gene expression in various optic nerve injuries including glaucoma. *Mol Vis* **19**, 2526-2541 (2013).

Levkovitch-Verbin, H., Vander, S., Makarovsky, D. & Lavinsky, F. Increase in retinal ganglion cells' susceptibility to elevated intraocular pressure and impairment of their endogenous neuroprotective mechanism by age. *Mol Vis* **19**, 2011-2022 (2013).

Li, G.-Y. & Osborne, N. N. Oxidative-induced apoptosis to an immortalized ganglion cell line is caspase independent but involves the activation of poly(ADP-ribose)polymerase and apoptosis-inducing factor. *Brain Res* **1188**, 35-43 (2008).

Libby, R. T. *et al.* Inherited glaucoma in DBA/2J mice: pertinent disease features for studying the neurodegeneration. *Vis Neurosci* **22**, 637-648 (2005).

Lingor, P. *et al.* ROCK inhibition and CNTF interact on intrinsic signalling pathways and differentially regulate survival and regeneration in retinal ganglion cells. *Brain* **131**, 250-263 (2008).

Liston, P. *et al.* Identification of XAF1 as an antagonist of XIAP anti-Caspase activity. *Nat Cell Bio* **3**, 128-133 (2001).

Liu, Z. *et al.* Structural basis for binding of Smac/DIABLO to the XIAP BIR3 domain. *Nature* **408**, 1004-1008 (2000).

Logan, A., Ahmed, Z., Baird, A., Gonzalez, A. M. & Berry, M. Neurotrophic factor synergy is required for neuronal survival and disinhibited axon regeneration after CNS injury. *Brain* **129**, 490-502 (2006).

Lu, M. *et al.* XIAP induces NF-KB activation via the BIR1/TAB1 interaction and BIR1 dimerization. *Mol Cell* **26**, 689-702 (2007).

Lütjen-Drecoll, E. Functional morphology of the trabecular meshwork in primate eyes. *Prog Ret Eye Res* **18**, 91-119 (1999).

Ma, Y. T., Hsieh, T., Forbes, M. E., Johnson, J. E. & Frost, D. 0. BDNF injected into the superior colliculus reduces developmental retinal ganglion cell death. *J Neurosci* **18**, 2097-2107 (1998).

MacFarlane, M., Merrison, W., Bratton, S. B. & Cohen, G. M. Proteasome-mediated degradation of Smac during apoptosis: XIAP promotes Smac ubiquitination in vitro. *J Biol Chem* **277**, 36611-36616 (2002).

Manasses, D. T. & Au, L. The new era of glaucoma micro-stent surgery. *Ophthalmol Ther* **5**, 135-146 (2016).

Martin, K. R. G., Quigley, H. A., Valenta, D., Kielczewski, J. & Pease, M. E. Optic nerve dynein motor protein distribution changes with intraocular pressure elevation in a rat model of glaucoma. *Exp Eye Res* **83**, 255-262 (2006).

Masland, R. H. The neuronal organization of the retina. *Neuron* **76**, 266-280 (2012).

McKinnon, S. J. *et al.* Baculoviral IAP repeat-containing-4 protects optic nerve axons in a rat glaucoma model. *Mol Ther* **5**, 780-787 (2002).

McMonnies, C. W. Glaucoma history and risk factors. *J Optom* **10**, 71-78 (2017).

Meyer-Franke, A., Kaplan, M. R., Pfrieger, F. W. & Barres, B. A. Characterization of the signaling interactions that promote the survival and growth of developing retinal ganglion cells in culture. *Neuron* **15**, 805-819 (1995).

Moreno, M. C. *et al.* Retinal oxidative stress induced by high intraocular pressure. *Free Radical Bio Med* **37**, 803-812 (2004).

Morrison, J. C. *et al.* A rat model of chronic pressure-induced optic nerve damage. *Exp Eye Res* **64**, 85- 96 (1997).

Müller, A., Hauk, T. G., Leibinger, M., Marienfeld, R. & Fischer, D. Exogenous CNTF stimulates axon regeneration of retinal ganglion cells partially via endogenous CNTF. *Mol Cell Neurosci* **41**, 233-246 (2009).

Neufeld, A. H., Hernandez, M. R. & Gonzalez, M. Nitric oxide synthase in the human glaucomatous optic nerve head. *Arch Ophthalmol* **115**, 497-503 (1997).

Nongpiur, M. E., Ku, J. Y. F. & Aung, T. Angle closure glaucoma: a mechanistic review. *Curr Opin Ophthalmol* **22**, 96-101 (2011).

Olney, J. *W. et al.* NMDA antagonist neurotoxicity: mechanism and prevention. *Science* **254**, 1515-1518 (1991).

Osborne, N. N. Pathogenesis of ganglion 'cell death' in glaucoma and neuroprotection: focus on ganglion cell axonal mitochondria. *Prog Brain Res* **173**, 339-352 (2008).

Parisi, V. Neural conduction in the visual pathways in ocular hypertension and glaucoma. *Graefes Arch Clin Exp Ophthalmol* **235**, 136-142 (1997).

Parisi, V., Miglior, S., Manni, G., Centofanti, M. & Bucci, M. G. Clinical ability of pattern electroretinograms and visual evoked potentials in detecting visual dysfunction in ocular hypertension and glaucoma. *Ophthalmology* **113**, 216-228 (2006).

Pease, M. E. *et al.* Effect of CNTF on retinal ganglion cell survival in experimental glaucoma. *Invest Ophthalmol Vis Sci* **50**, 2194-2200 (2009).

Pedersen, J., LaCasse, E. C., Seidelin, J. B., Coskun, M. & Nielsen, 0. H. Inhibitors of apoptosis (IAPs) regulate intestinal immunity and inflammatory bowel disease (IBD) inflammation. *Trends Mol Med* **20**, 652-665 (2014).

Peinado-Ramón, P., Salvador, M., Villegas-Perez, M. P. & Vidal-Sanz, M. Effects of axotomy and intraocular administration of NT-4, NT-3, and brain-derived neurotrophic factor on the survival of adult rat retinal ganglion cells. A quantitative in vivo study. *Invest Ophthalmol Vis Sci* **37**, 489-500 (1996).

Perígolo-Vicente, R. *et al.* IL-6, Al and A2aR: a crosstalk that modulates BDNF and induces neuroprotection. *Biochem Biophys Res Commun* **449**, 477-482 (2014).

Perlson, E., Maday, S., Fu, M.-M., Moughamian, A. J. & Holzbaur, E. L. F. Retrograde axonal transport: pathways to cell death? *Trends Neurosci* **33**, 335-344 (2010).

Porciatti, V. The mouse pattern electroretinogram. *Doc Ophthalmol* **115**, 145-153 (2007).

Quigley, H. A., Addicks, E. M., Green, W. R. & Maumenee, A. E. Optic nerve damage in human glaucoma. II. The site of injury and susceptibility to damage. *Arch Ophthalmol* **99**, 635-649 (1981).

Quigley, H. A. & Broman, A. T. The number of people with glaucoma worldwide in 2010 and 2020. *Br J Ophthalmol* **90**, 262-267 (2006).

Quigley, H. A., Hohman, R. M., Addicks, E. M., Massof, R. W. & Green, W. R. Morphologic changes in the lamina cribrosa correlated with neural loss in open-angle glaucoma. *Am J Ophthalmol* **95**, 673-691 (1983).

Quigley, H. A. *et al.* Retinal ganglion cell death in experimental glaucoma and after axotomy occurs by apoptosis. *Invest Ophthalmol Vis Sci* **36**, 774-786 (1995).

Quigley, H. A. *et al.* Retrograde axonal transport of BDNF in retinal ganglion cells is blocked by acute IOP elevation in rats. *Invest Ophthalmol Vis Sci* **41**, 3460-3466 (2000).

Renner, M. *et al.* Optic nerve degeneration after retinal ischemia/reperfusion in a rodent model. *Front Cell Neurosci* **11**, 254 (2017).

Renwick, J. *et al.* XIAP-mediated neuroprotection in retinal ischemia. *Gene Ther* **13**, 339-347 (2006).

Rezaie, T. *et al.* Adult-onset primary open-angle glaucoma caused by mutations in optineurin. *Science* **295**, 1077-1079 (2002).

Rudnicka, A. R., Mt-Isa, S., Owen, C. G., Cook, D. G. & Ashby, D. Variations in primary open-angle glaucoma prevalence by age, gender, and race: a Bayesian meta-analysis. *Invest Ophthalmol Vis Sci* **47**, 4254-4261 (2006).

Sappington, R. M., Carlson, B. J., Crish, S. D. & Calkins, D. J. The microbead occlusion model: a paradigm for induced ocular hypertension in rats and mice. *Invest Ophthalmol Vis Sci* **51**, 207-216 (2010).

Sathyamangalam, R. V. *et al.* Determinants of glaucoma awareness and knowledge in urban Chennai. *Indian I Ophthalmol* **57**, 355-360 (2009).

Sawai, H., Clarke, D. B., Kittlerova, P., Bray, G. M. & Aguayo, A. J. Brain-derived neurotrophic factor and neurotrophin-4/5 stimulate growth of axonal branches from regenerating retinal ganglion cells. *J Neurosci* **16**, 3887-3894 (1996).

Scott, F. L. *et al.* XIAP inhibits caspase-3 and -7 using two binding sites: evolutionarily conserved mechanism of IAPs. *EMBO J* **24**, 645-655 (2005).

Shields, M. B. Normal-tension glaucoma: is it different from primary open-angle glaucoma? *Curr Opin Ophthalmol* **19**, 85-88 (2008).

Shiozaki, E. N. *et al.* Mechanism of XIAP-mediated inhibition of caspase-9. *Mot Cell* **11**, 519-527 (2003).

Sinn, R. & Wittbrodt, J. An eye on eye development. *Mech Develop* **130**, 347-358 (2013).

Sisk, D. R. & Kuwabara, T. Histologic changes in the inner retina of albino rats following intravitreal injection of monosodium L-glutamate. *Graefes Arch Clin Exp Ophthalmol* **223**, 250-258 (1985).

Sofroniew, M. V. Molecular dissection of reactive astrogliosis and glial scar formation. *Trends Neurosci* **32**, 638-647 (2009).

Stehlik, C. *et al.* Nuclear factor (NF)-kappaB-regulated X-chromosome-linked iap gene expression protects endothelial cells from tumor necrosis factor alpha-induced apoptosis. *J Exp Med* **188**, 211-216 (1998).

Stone, E. M. *et al.* Identification of a gene that causes primary open angle glaucoma. *Science* **275**, 668-670 (1997).

Sucher, N. J., Lipton, S. A. & Dreyer, E. B. Molecular basis of glutamate toxicity in retinal ganglion cells. *Vision Res* **37**, 3483-3493 (1997).

Sun, C. *et al.* NMR Structure and mutagenesis of the third BIR domain of the inhibitor of apoptosis protein XIAP. *J Biol Chem* **275**, 33777-33781 (2000).

Sun, X. *et al.* Primary angle closure glaucoma: what we know and what we don't know. *Prog Ret Eye Res* **57**, 26-45 (2017).

Suzuki, Y., Nakabayashi, Y. & Takahashi, R. Ubiquitin-protein ligase activity of X-linked inhibitor of apoptosis protein promotes proteasomal degradation of caspase-3 and enhances its anti-apoptotic effect in Fas-induced cell death. *Proc Natl Acad Sci U S A* **98**, 8662-8667 (2001).

Takahashi, R. *et al.* A single BIR domain of XIAP sufficient for inhibiting caspases. *J Biol Chem* **273**, 7787-7790 (1998).

Tezel, G. & Yang, X. Caspase-independent component of retinal ganglion cell death, in vitro. *Invest Ophthalmol Vis Sci* **45**, 4049-4059 (2004).

Tezel, G., Yang, X. & Cai, J. Proteomic identification of oxidatively modified retinal proteins in a chronic pressure-induced rat model of glaucoma. *Invest Ophthalmol Vis Sci* **46**, 3177-3187 (2005).

Tham, Y.-C. *et al.* Global prevalence of glaucoma and projections of glaucoma burden through 2040: a systematic review and meta-analysis. *Ophthalmology* **121**, 2081-2090 (2014).

Thanos, S., Bähr, M., Barde, Y.–A., & Vanselow, J. Survival and axonal elongation of adult rat retinal ganglion cells. *Eur J Neurosci* **1**, 19-26 (1989).

Unoki, K & LaVail, M. M. Protection of the rat retina from ischemic injury by brain-derived neurotrophic factor, ciliary neurotrophic factor, and basic fibroblast growth factor. *Invest Ophthamol Vis Sci* **35**, 907-915 (1994).

Verhagen, A. M., Coulson, E. J. & Vaux, D. L. Inhibitor of apoptosis proteins and their relatives: IAPs and other BIRPs. *Genome Biol* **2**, REVIEWS3009 (2001).

Vithana, E. N. *et al.* Genome-wide association analyses identify three new susceptibility loci for primary angle closure glaucoma. *Nat Genet* **44**, 1142-1146 (2012).

Walsh, P., Kane, N. & Butler, S. The clinical role of evoked potentials. *J Neurol Neurosur Ps* **76**, ii16-ii22 (2005).

Wang, N., Chintala, S. K., Fini, M. E. and Schuman, J. S. Activation of a tissue-specific stress response in the aqueous outflow pathway of the eye defines the glaucoma disease phenotype. *Nat Med* **7**, 304-309 (2001).

Watson, P. G., Allen, E.D., Graham, C. M., Porter G. P. & Pickering, M. S. Argon laser trabeculoplasty or trabeculotomy: a prospective randomized block study. *Trans Ophthalmol Soc U K* **104** (Pt 1), 55-61 (1985).

Watts, M. T., Good, P. A. & O'neill, E. C. The flash stimulated VEP in the diagnosis of glaucoma. *Eye* **3**, 732-737 (1989).

Weinreb, R. N., Aung, T. & Medeiros, F. S. The pathophysiology and treatment of glaucoma. *JAMA* **311**, 1901-1911 (2014).

Weise, J. *et al.* Adenovirus-mediated expression of ciliary neurotrophic factor (CNTF) rescues axotomized rat retinal ganglion cells but does not support axonal regeneration in vivo. *Neurobiol Dis* **7**, 212-223 (2000).

Westphal, D., Dewson, G., Czabotar, P. E. & Kluck, R. M. Molecular biology of Bax and Bak activation and action. *BBA-Mol Cell Res* **1813**, 521-531 (2011).

Weymouth, A. E. & Vingrys, A. J. Rodent electroretinography: methods for extraction and interpretation of rod and cone responses. *Prog Ret Eye Res* **27**, 1-44 (2008).

Williams, P. A. *et al.* Neuroinflammation in glaucoma: a new opportunity. *Exp Eye Res* **157**, 20-27 (2017).

Wolfs, R. C. *et al.* Genetic risk of primary open-angle glaucoma: population-based familial aggregation study. *Arch Ophthalmol* **116**, 1640-1645 (1998).

Wong, W. W.-L. *et al.* cIAPs and XIAP regulate myelopoiesis through cytokine production in an RIPK1- and RIPK3-dependent manner. *Blood* **123**, 2562–2572 (2014).

Yabal, M. *et al.* XIAP Restricts TNF- and RIP3-dependent cell death and inflammasome activation. *Cell Rep* **7**, 1796–1808 (2014).

Yamaguchi, Y. & Miura, M. Programmed cell death in neurodevelopment. *Dev Cell* **32**, 478–490 (2015).

Yang, Y., Fang, S., Jensen, J. P., Weissman, A. M. & Ashwell, J. D. Ubiquitin protein ligase activity of IAPs and their degradation in proteasomes in response to apoptotic stimuli. *Science* **288**, 874–877 (2000).

Zadro-Lamoureux, L. A. *et al.* Effects on XIAP retinal detachment–induced photoreceptor apoptosis. *Invest Ophthalmol Vis Sci* **50**, 1448–1453 (2009).

Zolotukhin, S. *et al.* Production and purification of serotype 1, 2, and 5 recombinant adeno-associated viral vectors. *Methods* **28**, 158–167 (2002).